Optimal and robust control and estimation of linear paths to transition

By THOMAS R. BEWLEY¹ AND SHARON LIU²

¹Center for Turbulence Research, Stanford University, Stanford, CA 94305, USA ²Mechanical and Environmental Engineering Dept., UCSB, Santa Barbara, CA 93106, USA

(Received 30 September 1997 and in revised form 2 February 1998)

Optimal and robust control theories are used to determine effective, estimator-based feedback control rules for laminar plane channel flows that effectively stabilize linearly unstable flow perturbations at $Re=10\,000$ and linearly stable flow perturbations, characterized by mechanisms for very large disturbance amplification, at Re=5000. Wall transpiration (unsteady blowing/suction) with zero net mass flux is used as the control, and the flow measurement is derived from the wall skin friction. The control objective, beyond simply stabilizing any unstable eigenvalues (which is relatively easy to accomplish), is to minimize the energy of the flow perturbations created by external disturbance forcing. This is important because, when mechanisms for large disturbance amplification are present, small-amplitude external disturbance forcing may excite flow perturbations with sufficiently large amplitude to induce nonlinear flow instability.

The control algorithms used in the present work account for system disturbances and measurement noise in a rigorous fashion by application of modern linear control techniques to the discretized linear stability problem. The disturbances are accounted for both as uncorrelated white Gaussian processes (\mathcal{H}_2 or 'optimal' control) and as finite 'worst case' inputs which are maximally detrimental to the control objective (\mathcal{H}_{∞} or 'robust' control). Root loci and transient energy growth analyses are shown to be inadequate measures to characterize overall system performance. Instead, appropriately defined transfer function norms are used to characterize all systems considered in a consistent and relevant manner. In order to make a parametric study tractable in this high-dimensional system, a convenient new scaling to the estimation problem is introduced such that three scalar parameters $\{\gamma, \alpha, \ell\}$ may be individually adjusted to achieve desired closed-loop characteristics of the resulting systems. These scalar parameters may be intuitively explained, and are defined such that the resulting control equations retain the natural dual structure between the control parameter, ℓ , and the estimation parameter, α . The performance of the present systems with respect to these parameters is thoroughly investigated, and comparisons are made to simple proportional schemes where appropriate.

1. Introduction

The behaviour of small flow perturbations in simple laminar shear flows is an important and well-understood problem (Drazin & Reid 1981). As the Reynolds number is increased, laminar flows often become unstable and transition to turbulence occurs. The effects of the turbulence produced are very significant and often

undesirable, resulting in increased drag and heat transfer at flow boundaries. Thus, a natural engineering problem is to develop methods of flow control which can delay or eliminate transition to turbulence.

A firm theoretical basis for the control of small perturbations in viscous shear flows is only beginning to emerge. Some important steps in this direction, for the consideration of two-component (2C) disturbances, are provided by Hu & Bau (1994), Joshi, Speyer & Kim (1995, 1997), and Joslin et al. (1997). In these works, the eigenvalues of the linearized transition problem are successfully stabilized in a closed-loop framework such that the dynamics of the vertical velocity component of the flow acting in concert with the controller is considered. Hu & Bau (1994) examines a restricted class of multiple-input/multiple-output (MIMO) proportional controllers with a single controller gain, with skin friction as the measurement and wall temperature as the actuation. Joshi et al. (1997) examines a single-input/single-output (SISO) proportional-integral (PI) controller (i.e. a controller with both proportional and integral terms), with single-point skin friction measurements used to determine each sine-wave component of the distributed wall velocity actuation. Joshi et al. (1995) consider the \mathcal{H}_2 control of a problem related to the supercritical case presented here, reducing the problem to the nine least-stable modes in a Matlab implementation of an \mathcal{H}_2 controller, and make several interesting theoretical observations about the effects of the distributed nature of the problem at hand. A formal treatment of the distributed nature of the present problem is given by Bamieh (1997). Joslin et al. (1997) also apply \mathcal{H}_2 control theory to a problem related to the supercritical case presented here; in their approach, the control is determined through an adjoint formulation requiring full flowfield information.

Root loci, which partially characterize system behaviour by tracking the movement of closed-loop system *eigenvalues* as a function of control parameters (Joshi *et al.* 1995, 1997), are inadequate to quantify the performance of the present closed-loop systems, as they do not address the non-orthogonality of system *eigenvectors* (Trefethen *et al.* 1993). It is possible to characterize the non-orthogonality of a set of eigenvectors by determining the maximum transient energy growth of a stable system from a deleterious set of initial conditions by a variational formulation (Butler & Farrell 1992). However, such an approach is, at best, a dubious approximation of the method by which external disturbance forcing actually excites flow perturbations.

To adequately characterize the behaviour of a non-orthogonal linear system and its excitation by external disturbances, taking into account any known structure by which external disturbances force the state equation, transfer function norms are the appropriate measure (Skogestad & Postlethwaite 1996). In the present work, norms of the disturbance to state $(w \to x)$ transfer function and the disturbance to control $(w \to u)$ transfer function are introduced to quantify separately the response of the state and the response of the control to Gaussian and worst-case disturbances. For both of the cases considered, it is shown that the state response is significantly reduced in the closed-loop systems by application of modern control theory. Further, the r.m.s. of the control applied to achieve this reduced state response is bounded and may be kept small. On the other hand, the r.m.s. of controllers which contain a proportional component, such as that of Joshi et al. (1997), in response to Gaussian disturbances is shown to be unbounded.

The present work improves upon previous analyses of flow transition by rigorously accounting for state disturbances and measurement noise in both a Gaussian and a worst-case sense. The controllers and estimators used are determined by application of \mathcal{H}_2 ('optimal') and \mathcal{H}_∞ ('robust') approaches for linear problems. These techniques

have recently been put in a compact form by Doyle et al. (1989), and are shown to be well suited to the current problem.

A two-step control approach is used. First, a state estimate is developed from a (potentially inaccurate) model of the flow equations, with corrections to this state estimate provided by (noisy) flow measurements fed back through an estimator feedback matrix \boldsymbol{L} . This state estimate is then multiplied by a controller feedback matrix \boldsymbol{K} to determine the control. Control theory is used simply to compute the matrices \boldsymbol{K} and \boldsymbol{L} .

Potentially, this approach can yield better results than a proportional controller. In comparison to the SISO proportional approach, the present estimator-based approach has many more parameters in the control law (specifically, the elements of the matrices **K** and **L**), which are rigorously optimized for a clearly defined objective. In this manner, large multiple-input/multiple-output (MIMO) systems are handled naturally and the controller is coupled with an estimator which models the known dynamics of the system itself.

Classical control approaches, such as the PI controller of Joshi et al. (1997), are sufficient to stabilize any unstable eigenvalues in the present problems. However, modern (i.e. optimal and robust) control approaches produce closed-loop systems which are far less sensitive to external disturbances (as quantified in §6.1), and thus are far less likely to exhibit nonlinear instabilities when the external disturbance forcing is of finite magnitude. Many problems in fluid mechanics, including the later stages of transition and turbulence, are dominated by nonlinear behaviour. In such problems, the linear analysis performed in this paper is not valid. Iterative optimal control approaches over finite time intervals, which make use of full state information, may still be formulated (Abergel & Temam 1990) and performed (Moin & Bewley 1995) with impressive results. In order to make such schemes practical, one must understand how to account for disturbances in a rigorous fashion and how to estimate accurately the necessary components of the state (for instance, the location and strength of the near-wall coherent structures) based on limited flow measurements. The present paper makes these concepts clear in a fluid-mechanical sense, albeit for a linear problem, and thus provides a step in this development. Techniques to extend the robust control concept, introduced for problems in fluid mechanics in the present work, to nonlinear problems (such as turbulence) are discussed in Bewley, Moin & Temam (1997) and Bewley, Temam & Ziane (1998).

1.1. Outline of paper

The structure of the remainder of the paper is:

Section 2: the governing equations for the flow stability problem are put in a standard notation which makes subsequent application of control theory straightforward. Two specific cases are identified to be examined in detail: one supercritical and one subcritical.

Section 3: the control approach and numerical method used are briefly summarized. Section 4: the methods used to analyse the open-loop and closed-loop systems are reviewed.

Section 5: the uncontrolled ('open-loop') systems are studied in detail.

Section 6: the controlled ('closed-loop') systems are studied in detail. Root loci, which demonstrate the movement of the closed-loop system eigenvalues with respect to control parameters, are shown to illuminate some general trends, but fail to provide a quantitative measure of system performance. Maximum transient energy growth, which indicates non-orthogonality of closed-loop system eigenvectors, also fails to

provide a quantitative measure of system performance. The r.m.s. response of the state and the control to white Gaussian disturbances and 'worst-case' disturbances is ultimately quantified using the 2-norm and the ∞ -norm of the appropriate transfer functions, and the system behaviour as a function of the control parameters $\{\gamma, \alpha, \ell\}$ is thoroughly investigated.

Section 7: important results are summarized and concluding remarks are made.

2. Governing equations

In this Section, the equations governing small flow perturbations in a laminar channel flow (Poiseuille flow) are succinctly summarized in a form to which standard control techniques may be applied. This familiar discussion is presented to precisely define the problem under consideration, and to demonstrate that the simpler and more intuitive 'classical' derivation of the flow stability problem may be used easily in a controls setting, bypassing the involved stream function derivation of Joshi et al. (1995, 1997) which leads to a state-space formulation for two-component (2C) perturbations only. Readers interested only in how the control techniques are applied to the flow stability problem derived here are advised to proceed directly to §3.

In the present development, it is assumed that an array of sensors, which measure streamwise and spanwise skin friction, and actuators, which provide wall-normal blowing and suction with zero net mass flux, are mounted on the walls of a laminar channel flow. It is also assumed that a sufficient number of sensors and actuators is installed in both the streamwise and spanwise directions so that, in these directions, individual Fourier components of wall skin friction and wall transpiration may be approximated. The control analyses in the present work are then carried through for particular wavenumber pairs. The next natural step after the present work is to compute an array of controllers at an array of wavenumber pairs with the methods developed herein, then to inverse transform the resulting set of controllers back to the physical domain. Recent theoretical work by Bamieh (1997) indicates that such a procedure should result in spatial convolution kernels with compact support such that the weights on sensor measurements eventually decay exponentially as a function of distance from the actuator. This property will allow the convolution kernels to be truncated with a prescribed degree of accuracy at a finite distance from each actuator, resulting in implementable schemes in the physical domain. The present work sets the stage for this development.

2.1. Continuous form of flow equations

Consider a steady plane channel flow with maximum velocity U_0 and channel halfwidth δ . Non-dimensionalizing all velocities by U_0 and lengths by δ , the mean velocity profile in the streamwise direction (x) may be written $U(y) = 1 - y^2$ on the domain $y \in [-1, 1]$. The equations governing small, incompressible, three-dimensional perturbations $\{u, v, w, p\}$ to the mean flow U are given by the linearized Navier–Stokes and continuity equations

$$\dot{u} + U \frac{\partial}{\partial x} u + U'v = -\frac{\partial p}{\partial x} + \frac{1}{Re} \Delta u, \qquad (2.1a)$$

$$\dot{v} + U \frac{\partial}{\partial x} v = -\frac{\partial p}{\partial y} + \frac{1}{Re} \Delta v, \qquad (2.1b)$$

$$\dot{w} + U \frac{\partial}{\partial x} w = -\frac{\partial p}{\partial z} + \frac{1}{Re} \Delta w, \qquad (2.1c)$$

$$\dot{w} + U \frac{\partial}{\partial x} w = -\frac{\partial p}{\partial z} + \frac{1}{Re} \Delta w, \qquad (2.1c)$$

$$\frac{\partial u}{\partial x} + \frac{\partial v}{\partial y} + \frac{\partial w}{\partial z} = 0, (2.2)$$

where $\Delta \equiv \partial^2/\partial x^2 + \partial^2/\partial y^2 + \partial^2/\partial z^2$ is the Laplacian, $Re \equiv U_0 \delta/v$ is the Reynolds number, v is the kinematic viscosity, dot (') denotes $\partial/\partial t$, and prime (') denotes d/dy. A single equation for the normal component of velocity v, found by taking the Laplacian of (2.1b), substituting for Δp from the divergence of (2.1), and applying (2.2), is

$$\Delta \dot{v} = \left\{ -U \frac{\partial}{\partial x} \Delta + U' \frac{\partial}{\partial x} + \Delta (\Delta/Re) \right\} v. \tag{2.3a}$$

The equation for the normal component of vorticity $\omega \equiv \partial u/\partial z - \partial w/\partial x$, found by subtracting $\partial/\partial x$ of (2.1c) from $\partial/\partial z$ of (2.1a), is

$$\dot{\omega} = \left\{ -U' \frac{\partial}{\partial z} \right\} v + \left\{ -U \frac{\partial}{\partial x} + \Delta / Re \right\} \omega. \tag{2.3b}$$

The flow perturbation problem in $\{u, v, w, p\}$ with second-order partial derivatives in (2.1)–(2.2) has been reduced to a problem in $\{v, \omega\}$ with fourth-order partial derivatives in (2.3) with no loss of generality; essentially, the three-component velocity field has been projected onto a two-component divergence-free manifold by eliminating the pressure from the equations and applying continuity. Such a manipulation is standard practice for both the present derivation (Gustavsson & Hultgren 1980) and the fully nonlinear Navier–Stokes equation (Kim, Moin & Moser 1987).

As the domain is homogeneous in the *x*- and *z*-directions, we may Fourier transform the solution such that

$$v(x, y, z, t) = \sum_{k_x, k_z} \hat{v}(k_x, y, k_z, t) \exp[i(k_x x + k_z z)],$$

$$\omega(x, y, z, t) = \sum_{k_x, k_z} \hat{\omega}(k_x, y, k_z, t) \exp[i(k_x x + k_z z)].$$

As the various Fourier modes are orthogonal and equations (2.3a) and (2.3b) are linear, the solution for each wavenumber pair (k_x, k_z) is decoupled and obeys the equations

$$\Delta \dot{v} = \{-i k_x U \Delta + i k_x U' + \Delta(\Delta/Re)\} v \tag{2.4a}$$

$$\dot{\omega} = \{-ik_z U'\} v + \{-ik_x U + \Delta/Re\} \omega, \tag{2.4b}$$

where the hat accents (^) have been dropped for notational convenience and the Laplacian now takes the form $\Delta \equiv \partial^2/\partial y^2 - k_x^2 - k_z^2$. Equation (2.4a) is the well-known (fourth-order) Orr-Sommerfeld equation for the wall-normal velocity modes, and (2.4b) is the (second-order) equation for the wall-normal vorticity modes. Note the one-way coupling between these two equations. Also note that, from any solution $\{v,\omega\}$, the values of u and w may be extracted by manipulation of the above equations into the forms

$$u = \frac{i}{k_x^2 + k_z^2} \left(k_x \frac{\partial v}{\partial y} - k_z \, \omega \right) \quad \text{and} \quad w = \frac{-i}{k_x^2 + k_z^2} \left(k_z \, \frac{\partial v}{\partial y} - k_x \, \omega \right), \tag{2.5}$$

and p may be found by solution of the equation $\Delta p = -2i k_x U' v$. Control is applied at the wall as a boundary condition on the wall-normal component of velocity v. The boundary conditions on u and w are no-slip (u = w = 0), which implies that, at the wall, $\omega = 0$ and (by continuity) $\partial v/\partial y = 0$.

2.2. Discrete form of flow equations

The continuous equations for the $\{v,\omega\}$ perturbations in (2.4) are now discretized on a grid of N+1 Chebyshev–Gauss–Lobatto points in the wall-normal direction such that

$$y_{\kappa} = \cos(\pi \kappa / N)$$
 for $0 \le \kappa \le N$.

An $(N+1) \times (N+1)$ matrix \mathcal{D} may be expressed (Canuto *et al.* 1988, equation 2.4.31) such that the derivative of ω with respect to y on the discrete set of N+1 points is given by

$$\omega' = \mathcal{D} \omega$$
 and $\omega'' = \mathcal{D} \omega'$.

where the prime (') indicates the derivative of the vector ω with respect to y. The homogeneous Neumann boundary condition on v is accomplished by modifying the first derivative matrix such that

$$\tilde{\mathscr{D}}_{\iota \kappa} = \begin{cases} 0, & \iota = 0, N \\ \mathscr{D}_{\iota \kappa}, & 1 \leqslant \iota \leqslant N - 1. \end{cases}$$

Differentiation of v with respect to v is then given by

$$\mathbf{v}' = \tilde{\mathscr{D}}\mathbf{v}, \quad \mathbf{v}'' = \mathscr{D}\mathbf{v}', \quad \mathbf{v}''' = \mathscr{D}\mathbf{v}'' \quad \text{and} \quad \mathbf{v}'''' = \mathscr{D}\mathbf{v}'''.$$

With these derivative matrices, it is straightforward to write (2.4) in matrix form. This is accomplished by first expressing the matrix form of (2.4) on all N+1 collocation points such that

$$\dot{\mathbf{v}} = \mathcal{L}\mathbf{v},\tag{2.6a}$$

$$\dot{\boldsymbol{\omega}} = \mathscr{C} \boldsymbol{v} + \mathscr{S} \boldsymbol{\omega}, \tag{2.6b}$$

where the $(N+1) \times (N+1)$ matrices \mathcal{L} , \mathcal{C} , and \mathcal{L} represent the spatial discretization of the bracketed operations in (2.4). The Dirichlet boundary conditions are explicitly prescribed as separate 'forcing' terms. To accomplish this, decompose \mathcal{L} , \mathcal{C} , and \mathcal{L} according to

$$\mathscr{L} = \begin{pmatrix} * & * & * \\ \pmb{b}_{11} & \mathscr{L}_c & \pmb{b}_{12} \\ * & * & * \end{pmatrix}, \quad \mathscr{C} = \begin{pmatrix} * & * & * \\ \pmb{b}_{21} & \mathscr{C}_c & \pmb{b}_{22} \\ * & * & * \end{pmatrix}, \quad \mathscr{S} = \begin{pmatrix} * & * & * \\ * & \mathscr{S}_c & * \\ * & * & * \end{pmatrix},$$

where \mathscr{L}_c , \mathscr{C}_c , and \mathscr{S}_c are $(N-1)\times (N-1)$ and \boldsymbol{b}_{11} , \boldsymbol{b}_{12} , \boldsymbol{b}_{21} , and \boldsymbol{b}_{22} are $(N-1)\times 1$. Noting that $\omega_0 = \omega_N = 0$ by the no-slip condition, and defining

$$m{x} \equiv egin{pmatrix} v_1 \\ drappoondows \\ v_{N-1} \\ drappoondows \\ drappoondows \\ \omega_{N-1} \end{pmatrix}, \quad m{A} \equiv egin{pmatrix} & m{\mathcal{L}}_c & m{0} \\ & & & \\ &$$

† Note that, for $k_x^2 + k_z^2 \neq 0$, the matrix form of the left-hand side of (2.4a) is invertible, so the form (2.6a) is easily determined.

where x is $2(N-1) \times 1$, \boldsymbol{A} is $2(N-1) \times 2(N-1)$, \boldsymbol{B} is $2(N-1) \times 2$, and \boldsymbol{u} is 2×1 , we may express (2.6) in the form

The vector \mathbf{x} , which contains the normal velocity fluctuations v_i and normal vorticity fluctuations ω_i at the grid points on the interior of the channel, is referred to as the 'state'. The vector \mathbf{u} , which contains the blowing/suction velocity at the top and bottom walls, is referred to as the 'control'.

2.3. Wall measurements

We will consider control algorithms using both full flowfield information and wall information only. For the latter case, we will assume that measurements made at the wall provide information about the streamwise and spanwise skin friction, from which (subtracting out the known influence of $\partial v/\partial x$ and $\partial v/\partial z$ from the stress tensor at the wall) we may determine the following four quantities:

$$y_{m1} = -\frac{1}{Re} \frac{\partial u}{\partial y} \Big|_{upper \ wall}, \quad y_{m2} = \frac{1}{Re} \frac{\partial u}{\partial y} \Big|_{lower \ wall},$$

$$y_{m3} = -\frac{1}{Re} \frac{\partial w}{\partial y} \Big|_{upper \ wall}, \quad y_{m4} = \frac{1}{Re} \frac{\partial w}{\partial y} \Big|_{lower \ wall}.$$
(2.8)

With (2.5), we may express these measurements as linear combinations of v and ω . Defining $a \equiv i k_x/(k_x^2 + k_z^2)/Re$ and $b \equiv -i k_z/(k_x^2 + k_z^2)/Re$, the measurements are expressed in terms of the discrete vectors \mathbf{v} and $\boldsymbol{\omega}$ as

$$y_{m1} = (-a \mathcal{D} \tilde{\mathcal{D}} \mathbf{v} - b \mathcal{D} \boldsymbol{\omega}) \Big|_{upper \ wall}, \quad y_{m2} = (a \mathcal{D} \tilde{\mathcal{D}} \mathbf{v} + b \mathcal{D} \boldsymbol{\omega}) \Big|_{lower \ wall},$$
$$y_{m3} = (-b \mathcal{D} \tilde{\mathcal{D}} \mathbf{v} - a \mathcal{D} \boldsymbol{\omega}) \Big|_{upper \ wall}, \quad y_{m4} = (b \mathcal{D} \tilde{\mathcal{D}} \mathbf{v} + a \mathcal{D} \boldsymbol{\omega}) \Big|_{lower \ wall}.$$

Decompose \mathcal{D} , $\tilde{\mathcal{D}}$, and $(\mathcal{D}\tilde{\mathcal{D}})$ according to

$$\mathscr{D} = \begin{pmatrix} * & c_3 & * \\ * & * & * \\ * & c_4 & * \end{pmatrix}, \quad \tilde{\mathscr{D}} = \begin{pmatrix} * & * & * \\ * & \tilde{\mathscr{D}}_c & * \\ * & * & * \end{pmatrix}, \quad (\mathscr{D}\tilde{\mathscr{D}}) = \begin{pmatrix} d_1 & c_1 & d_3 \\ * & * & * \\ d_2 & c_2 & d_4 \end{pmatrix},$$

where $\tilde{\mathcal{D}}_c$ (to be used in the following section) is $(N-1) \times (N-1)$, c_1 , c_2 , c_3 , and c_4 are $1 \times (N-1)$, and d_1 , d_2 , d_3 , and d_4 are 1×1 . Finally, defining

$$\mathbf{y}_{m} \equiv \begin{pmatrix} y_{m1} \\ y_{m2} \\ y_{m3} \\ y_{m4} \end{pmatrix}, \quad \mathbf{C} \equiv \begin{pmatrix} -a \, \mathbf{c}_{1} & -b \, \mathbf{c}_{3} \\ a \, \mathbf{c}_{2} & b \, \mathbf{c}_{4} \\ -b \, \mathbf{c}_{1} & -a \, \mathbf{c}_{3} \\ b \, \mathbf{c}_{2} & a \, \mathbf{c}_{4} \end{pmatrix}, \quad \mathbf{D} \equiv \begin{pmatrix} a \, d_{1} & -a \, d_{3} \\ -a \, d_{2} & a \, d_{4} \\ b \, d_{1} & -b \, d_{3} \\ -b \, d_{2} & b \, d_{4} \end{pmatrix},$$

where y_m is 4×1 , **C** is $4 \times 2(N-1)$, and **D** is 4×2 , allows us to express y_m in the form of a linear combination of the state x and the control u

$$y_m = \mathbf{C}x + \mathbf{D}u. \tag{2.9}$$

The vector y_m is referred to as the 'measurement'.

2.4. Inner product, vector 2-norm, and energy density

Define the inner product for two discrete vectors \boldsymbol{u} and \boldsymbol{v} discretized on the collocation points $y_{\kappa} = \cos(\pi \kappa/N)$ by

$$(\boldsymbol{u},\,\boldsymbol{v}) \equiv \sum_{\kappa=0}^{N} u_{\kappa}^{*} v_{\kappa} \, \zeta_{\kappa}, \quad \text{where} \quad \zeta_{\kappa} \equiv \begin{cases} \frac{\pi}{2N}, & \kappa=0,N \\ \frac{\pi}{N}, & 1 \leqslant \kappa \leqslant N-1. \end{cases}$$

Orthogonality of two vectors implies that their inner product is zero, (u, v) = 0. The 2-norm of a vector u, denoted ||u||, is defined as the square root of (u, u). Note that, for two vectors of the same dimension as the state vector x, which is defined only on the interior grid points, the inner product is given simply by

$$(\boldsymbol{u},\,\boldsymbol{v}) = \frac{\pi}{N}\,\boldsymbol{u}^*\,\boldsymbol{v},\tag{2.10}$$

where star (*) applied to a vector denotes conjugate transpose. The corresponding inner product for two continuous complex functions u, v on the domain $y \in [-1, 1]$ is given by

$$(u, v) \equiv \int_{-1}^{1} u^* v \, \eta \, dy$$
, where $\eta(y) \equiv (1 - y^2)^{-1/2}$

and the star (*) denotes the complex conjugate. For sufficiently smooth functions u, v on a sufficiently large number N of Chebyshev–Gauss–Lobatto grid points (Canuto et al. 1988), this inner product of the continuous functions approximates the inner product of the discrete vectors, $(u, v) \approx (u, v)$. The implication of using a discretization-dependent weighting factor, such as $\eta(y)$, to develop a control rule is discussed in § 6.2.

For the purpose of developing control rules, the kinetic energy density is a more physically relevant quantity than measures derived from a (discretization-dependent) 2-norm of the discretized vector, such as that given by $\eta(y)$ above. The kinetic energy density of a flow perturbation in the physical domain is

$$\mathscr{E} = \frac{1}{V} \int_{-1}^{1} \int_{0}^{2\pi/k_x} \int_{0}^{2\pi/k_z} \frac{u^2 + v^2 + w^2}{2} \, \mathrm{d}z \, \mathrm{d}x \, \mathrm{d}y,$$

where $V = 8\pi/(k_x k_z)$ is the volume of the domain under consideration. Considering a single Fourier mode (k_x, k_z) and (again) dropping the hat accents (^) for notational convenience, the kinetic energy density is expressed in terms of $\{\hat{v}, \hat{\omega}\}$ as

$$\mathscr{E} = \frac{1}{8} \int_{-1}^{1} \left[v^* v + \frac{1}{k_v^2 + k_z^2} \left(\frac{\partial v^*}{\partial v} \frac{\partial v}{\partial y} + \omega^* \omega \right) \right] dy.$$

For the discrete state vector x, this integration corresponds to

and Ω is an $(N-1) \times (N-1)$ diagonal matrix with nonzero entries $\Omega_{\kappa\kappa} = \zeta_{\kappa}/\eta(y_{\kappa})$, where $1 \le \kappa \le N-1$, to properly account for the integrations on the stretched mesh.

2.5. Cases studied

It is well known that, for supercritical Re > 5772, the uncontrolled problem is linearly unstable, with the most unstable modes occurring for flow perturbations with $k_z \approx 0$, and that, for subcritical $Re \leq 5772$, the uncontrolled problem is linearly stable. However, transition often occurs at a Reynolds number well below that required for linear instability of the laminar flow. Butler & Farrell (1992) show that the non-orthogonality of the eigenmodes of subcritical flows, especially for flow perturbations with $k_x \approx 0$, implies that flow perturbations of a particular initial structure will experience large, O(Re) amplification of energy before their eventual decay. They suggest that such transient linear amplification can sometimes lead to flow perturbations large enough for nonlinear instability to be triggered, if such initial conditions ever happen to be encountered. This paper will explore control techniques which simultaneously (a) stabilize any unstable system eigenvalues, and (b) greatly reduce the maximum transient energy growth of small flow perturbations due to nonorthogonal system eigenvectors. The quantitative comparison of the various controlled closed-loop systems, however, will finally be obtained by the transfer function analysis to be described in §4.4.

To simplify our discussion, we will restrict our attention in the remainder of this work to one supercritical case and one subcritical case:

Case (i)
$$Re = 10000, k_x = 1, k_z = 0;$$

Case (ii) $Re = 5000, k_x = 0, k_z = 2.044.$

Case (i), which is supercritical, is the 'classic' $Re = 10\,000$ case benchmarked by Orszag (1971). It has been studied by several authors since, including Joshi *et al.* (1997). Case (ii), which is subcritical, is the wavenumber pair that gives the maximum transient energy growth at Re = 5000, as shown by Butler & Farrell (1992).

For case (i), $k_z = 0$ and thus $\mathscr{C} = \mathbf{0}$ in (2.6), entirely decoupling the $\boldsymbol{\omega}$ eigenmodes from both the \boldsymbol{v} eigenmodes and from the control $\boldsymbol{u} = (v_0, v_N)^T$. The $\boldsymbol{\omega}$ eigenmodes are thus unaffected by the application of the control \boldsymbol{u} . Fortunately, it is also found that the $\boldsymbol{\omega}$ eigenmodes are stable. Thus, for the purpose of studying the effect of the control in case (i) (only), we may restrict our attention to the \boldsymbol{v} eigenmodes according to a reduced system with

$$m{x} \equiv egin{pmatrix} v_1 \\ dots \\ v_{N-1} \end{pmatrix}, \quad m{A} \equiv egin{pmatrix} & \mathcal{L}_c & \\ & & \end{pmatrix}, \quad m{B} \equiv egin{pmatrix} -m{b}_{11} & m{b}_{12} \\ & & \end{pmatrix}, \quad m{u} \equiv egin{pmatrix} -v_0 \\ v_N \end{pmatrix},$$

where x is $(N-1) \times 1$, A is $(N-1) \times (N-1)$, B is $(N-1) \times 2$, and u is 2×1 , and

$$\mathbf{y}_{m} \equiv \begin{pmatrix} y_{m1} \\ y_{m2} \\ y_{m3} \\ y_{m4} \end{pmatrix}, \quad \mathbf{C} \equiv \begin{pmatrix} -a \, \mathbf{c}_{1} \\ a \, \mathbf{c}_{2} \\ -b \, \mathbf{c}_{1} \\ b \, \mathbf{c}_{2} \end{pmatrix}, \quad \mathbf{D} \equiv \begin{pmatrix} a \, d_{1} & -a \, d_{3} \\ -a \, d_{2} & a \, d_{4} \\ b \, d_{1} & -b \, d_{3} \\ -b \, d_{2} & b \, d_{4} \end{pmatrix},$$

where y_m is 4×1 , **C** is $4 \times (N-1)$, and **D** is 4×2 . The full dynamics of the controlled system for case (i) is simply the dynamics of the controlled reduced system for v together with the decoupled, stable dynamics of the uncontrolled system for ω .

For case (ii), as $\mathscr{C} \neq \mathbf{0}$, we must use the full coupled system derived in §2.2 and §2.3. Note that case (ii), which consists of three-component $\{u, v, w\}$ perturbations, varies only in the y- and z-directions, and therefore is properly referred to (Reynolds & Kassinos 1995) as 2D, 3C (two-dimensional, three-component). Case (i), for which

we consider only the two-component $\{u, v\}$ perturbations, varies only in the x- and y-directions, and therefore is referred to as 2D, 2C (two-dimensional, two-component).

2.6. State disturbances and measurement noise

State disturbances of some level are inevitable in any flow. They arise from sources such as acoustics, surface irregularities, vibrations of the wind-tunnel walls, etc. Measurement noise of some level is also inevitable. It arises from inaccuracies of the sensors and from the electronics processing their signals. These phenomena are now accounted for in a general form. The simple assumptions used to solve the problem here may be refined as more information is learned about particular flows of interest.

Define \mathbf{G}_1 as the square root of the expected covariance of the state disturbances to be added to (2.7) and \mathbf{G}_2 as the square root of the expected covariance of measurement noise to be added to (2.9). Note that \mathbf{G}_1 and \mathbf{G}_2 are time invariant, and it can be assumed that \mathbf{G}_2 is non-singular due to the inevitability of noise in measurements. In the present problem, as nothing yet is known about the state disturbances or measurement noise *a priori*, they are assumed to have the simple covariances

$$\mathbf{G}_1 \equiv \mathbf{I}$$
 and $\mathbf{G}_2 \equiv \alpha \mathbf{I} \Rightarrow \alpha \mathbf{G}_2^{-1} = \mathbf{I}$.

The parameter α^2 is defined as the ratio of the maximum singular value, σ_{max} , of the covariance of the measurement noise to the maximum singular value of the covariance of the state disturbances,

$$lpha^2 \equiv rac{\sigma_{max}(\mathbf{G}_2^2)}{\sigma_{max}(\mathbf{G}_1^2)},$$

and the problem is normalized such that $\sigma_{max}(\mathbf{G}_1^2) = 1$. Known structure of these covariances (for example, if one sensor is known to be noisier than another) is accounted for by replacing the identity matrices in the above expressions with appropriate matrices of unit maximum singular value, retaining the quantity α to reflect the balance between the magnitudes of the two types of disturbances.

The disturbed system under consideration may be written

$$\dot{x} = \mathbf{A}x + \mathbf{G}_1 \mathbf{w}_1 + \mathbf{B}\mathbf{u},$$

$$y_m = \mathbf{C}x + \mathbf{G}_2 \mathbf{w}_2 + \mathbf{D}\mathbf{u}.$$

The controllers developed in this work will rigorously account for the state disturbances G_1w_1 and the measurement noise G_2w_2 . These 'disturbances', as they shall generically be referred to, are considered both in a Gaussian sense and in a worst-case sense; the present system definition is convenient for the consideration of both types of disturbances.

When optimizing the system response to disturbances with a Gaussian structure, as any covariance of the disturbances known in advance is accounted for in G_1 and G_2 , the external signals w_1 and w_2 are taken as uncorrelated, zero-mean, white Gaussian processes with covariance $E[w_1 w_1^*] = I$, $E[w_2 w_2^*] = I$. Note that, for the present system, the expectation value may be written

$$E[\cdot] = \lim_{T \to \infty} \frac{1}{T} \int_0^T [\cdot] \, \mathrm{d}t.$$

† This scaling of the problem is used because it turns out to be quite convenient in the derivation of the \mathcal{H}_{∞} estimator in the development to follow. Note that the definition of α is based on the ratio of maximum singular values of the covariance matrices; the maximum singular value is also referred to as the induced matrix 2-norm, i.e. $||\mathbf{G}_2^2||_2 \equiv \sigma_{max}(\mathbf{G}_2^2)$.

When optimizing the system response to worst-case disturbances, as, again, any covariance of the disturbances known in advance is accounted for in \mathbf{G}_1 and \mathbf{G}_2 , no disturbance structure is assumed at all. Instead, a finite 'unstructured' disturbance is found which maximizes a cost function representing the control objective. Simultaneously, a controller is found which minimizes the same cost function in the presence of this disturbance. This is the essence of non-cooperative game theory, and will be discussed further in § 3.

To account for disturbances in a more tractable manner in the control theory, define a new 'observation' vector y by a simple change of variables such that

$$y \equiv \alpha \mathbf{G}_2^{-1}(y_m - \mathbf{D} \mathbf{u}).$$

The observation y is easily determined from the flow measurements. Also, define

$$\mathbf{B}_1 \equiv \begin{pmatrix} \mathbf{G}_1 & \mathbf{0} \end{pmatrix}, \quad \mathbf{B}_2 \equiv \mathbf{B}, \quad \mathbf{C}_2 \equiv \alpha \, \mathbf{G}_2^{-1} \mathbf{C}, \quad \mathbf{D}_{21} \equiv \begin{pmatrix} \mathbf{0} & \alpha \, \mathbf{I} \end{pmatrix}, \quad \mathbf{w} \equiv \begin{pmatrix} \mathbf{w}_1 \\ \mathbf{w}_2 \end{pmatrix}.$$

The system is then written in the standard form

$$\begin{vmatrix}
\dot{x} = \mathbf{A} x + \mathbf{B}_1 w + \mathbf{B}_2 u, \\
y = \mathbf{C}_2 x + \mathbf{D}_{21} w.
\end{vmatrix} (2.11)$$

3. Application of control theory and numerical method

3.1. Summary of control approach

In § 2, it was shown that the equations governing small flow perturbations in a laminar channel flow may be expressed in the standard form

$$\dot{x} = \mathbf{A} x + \mathbf{B}_1 w + \mathbf{B}_2 u, \tag{3.1a}$$

$$y = \mathbf{C}_2 x + \mathbf{D}_{21} w. \tag{3.1b}$$

A simple method is sought to 'close the loop' to stabilize the system; i.e. to determine a control u based on the observations y to force the state x towards zero in a manner which rigorously accounts for the disturbances w. A system model with a structure similar to the system (3.1) itself, but without the influence of the unknown disturbances, is used for this purpose such that

$$\dot{\hat{x}} = \mathbf{A}\,\hat{x} + \mathbf{B}_2\mathbf{u} - \hat{\mathbf{u}},\tag{3.2a}$$

$$\hat{\mathbf{v}} = \mathbf{C}_2 \hat{\mathbf{x}},\tag{3.2b}$$

with feedback \hat{u} based on the difference between the observations of the state y and the corresponding quantity in the model \hat{y} such that

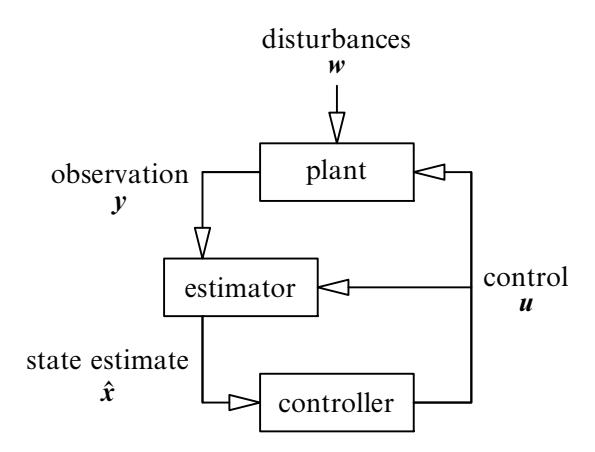
$$\hat{\boldsymbol{u}} = \boldsymbol{\mathsf{L}}(\boldsymbol{\mathsf{y}} - \hat{\boldsymbol{\mathsf{y}}}). \tag{3.2c}$$

The control u, in turn, is based on the state estimate \hat{x} such that

$$u = K\hat{x}. \tag{3.3}$$

Equation (3.1), is referred to as the 'plant', (3.2) is referred to as the 'estimator', and (3.3) is referred to as the 'controller'. The problem at hand is to compute linear time-invariant (LTI) matrices \boldsymbol{L} and \boldsymbol{K} such that (i) the estimator feedback $\hat{\boldsymbol{u}}$ forces the state estimate $\hat{\boldsymbol{x}}$ in the estimator towards the state \boldsymbol{x} in the plant, and (ii) the controller feedback \boldsymbol{u} forces the state \boldsymbol{x} towards zero in the plant.

The flow of information is illustrated schematically in the following block diagram.



The plant, forced by external disturbances, has an internal state x which cannot be observed. Instead, a noisy observation y is made and an estimate of the state \hat{x} determined. This state estimate is then fed through the controller to determine the control u to be applied on the plant to regulate x to zero.

Several recent references describe in detail how \mathcal{H}_2 ('optimal') and \mathcal{H}_{∞} ('robust') techniques determine L and K for systems of the form (3.1)–(3.3) in the presence of structured and unstructured disturbances w. The reader is referred in particular to Doyle et al. (1989), Dailey et al. (1990), Green & Limebeer (1995), and Zhou, Doyle & Glover (1996) for further discussion of these control theories, and Bewley & Agarwal (1996) for a tutorial in the context of the current problem. To summarize briefly, a cost function $\mathcal J$ describing the control problem at hand is defined that weighs together the state x, the control u, and the disturbance w such that

$$\mathscr{J} \equiv E\left[x^* \mathbf{Q} x + \ell^2 u^* u - \gamma^2 w^* w\right] = E\left[z^* z - \gamma^2 w^* w\right], \tag{3.4a}$$

where

$$z = \mathbf{C}_1 x + \mathbf{D}_{12} \mathbf{u} \tag{3.4b}$$

with

$$oldsymbol{c}_1 \equiv egin{pmatrix} oldsymbol{Q}^{1/2} \ oldsymbol{0} \end{pmatrix}, \quad oldsymbol{D}_{12} \equiv egin{pmatrix} oldsymbol{0} \ \ell \, oldsymbol{I} \end{pmatrix}.$$

This cost function is minimized with respect to the control \boldsymbol{u} and maximized with respect to the disturbance \boldsymbol{w} . For sufficiently large γ and a stabilizable, detectable system (as defined in §4.1), this results in finite values for both \boldsymbol{u} and \boldsymbol{w} , the magnitudes of which are governed by the three scalars $\{\gamma,\alpha,\ell\}$. Recall that α^2 , defined earlier, quantifies the relative level to which the observation \boldsymbol{y} is corrupted by measurement noise.

The parameter ℓ^2 may be interpreted as the 'price' of the control. The $\ell \to \infty$ limit, which corresponds to 'expensive control', results in the smallest possible u which stabilizes the system, i.e. makes $E[x^*Qx]$ finite. Reduced values of ℓ penalize the cost function less upon the application of control, and thereby tend to result in a larger control magnitude $E[u^*u]$ and a smaller energy density of the state $E[x^*Qx]$.

Consider the min/max problem just described as a differential game between a fluid dynamicist seeking the 'best' control u which stabilizes the flow perturbation with limited control effort and nature seeking the 'maximally malevolent' small disturbance w which destabilizes the flow perturbation (Green & Limebeer 1995, p. 218). The parameter γ^2 factors into such a competition as a weighting on the magnitude of the disturbance which nature can afford to offer, in a manner analogous to the parameter ℓ^2 , which is a weighting on the magnitude of the control which the fluid dynamicist can afford to offer. The negative sign on the term involving γ^2 is necessary because the cost function is maximized with respect to the disturbance w, while it is minimized with respect to the control u. The $\gamma \to \infty$ limit, referred to as the \mathcal{H}_2 solution, removes the disturbance 'player' from the non-cooperative game between u and w(i.e. $w \to 0$ in the maximization). This limit may also be interpreted as assuming the disturbance w is white and uncorrelated with the control applied, i.e. $E[w w^*] = I$ and $E[w u^*] = 0$, which implies that the problems of control and estimation in the \mathcal{H}_2 limit are decoupled. Reduced values of γ introduce a 'maximally malevolent' disturbance w of increased magnitude relative to the magnitude of the control u.

Solving for the feedback which is effective even in the presence of such malevolent disturbances achieves system robustness. In the present systems, for $\gamma < \gamma_0$ for some critical value γ_0 (which may be found by trial and error), the non-cooperative game does not have a finite solution; essentially, nature wins. The feedback corresponding to $\gamma = \gamma_0$ results in a stable system even when nature is on the brink of making the system unstable. This is sometimes referred to as the 'optimal' \mathcal{H}_{∞} feedback, as it is the feedback which is 'most robust'. However, the 'optimal' \mathcal{H}_{∞} feedback is generally not the most suitable choice overall, as discussed in §6.1.1 and §6.1.2.

The parameter γ in the min/max problem formulated above in the time domain is also, it turns out, an upper bound on the ∞ -norm of the transfer function from the disturbance w to the performance measure z in the frequency domain, defined precisely in §4.4 and denoted $||T_{zw}||_{\infty}$ (Zhou *et al.* 1996). Thus, by reducing γ to the minimum values possible (γ_0) when computing the estimator feedback matrix L and the controller feedback matrix K, the most restrictive bounds on $||T_{zw}||_{\infty}$ in the resulting closed-loop systems are attained.

An estimator/controller which minimizes \mathcal{J} in the presence of that disturbance which simultaneously maximizes \mathcal{J} is given by the estimator feedback

$$\mathbf{L} = -\frac{1}{\alpha^2} \mathbf{Y} \mathbf{C}_2^*, \text{ where } \mathbf{Y} = \text{Ric} \begin{pmatrix} \mathbf{A}^* & \frac{1}{\gamma^2} \mathbf{C}_1^* \mathbf{C}_1 - \frac{1}{\alpha^2} \mathbf{C}_2^* \mathbf{C}_2 \\ -\mathbf{B}_1 \mathbf{B}_1^* & -\mathbf{A} \end{pmatrix}, (3.5)$$

and the controller feedback

$$\mathbf{K} = -\frac{1}{\ell^2} \mathbf{B}_2^* \mathbf{X}, \quad \text{where} \quad \mathbf{X} = \text{Ric} \begin{pmatrix} \mathbf{A} & \frac{1}{\gamma^2} \mathbf{B}_1 \mathbf{B}_1^* - \frac{1}{\ell^2} \mathbf{B}_2 \mathbf{B}_2^* \\ -\mathbf{C}_1^* \mathbf{C}_1 & -\mathbf{A}^* \end{pmatrix}, \quad (3.6)$$

where Ric(·) denotes the solution of the associated Riccati problem (Doyle *et al.* 1989). Standard numerical techniques to solve equations of this form are well developed (Laub 1991). Solutions to these Riccati problems exist only for sufficiently large γ at given values of ℓ and α . As previously stated, the smallest $\gamma = \gamma_0$ for which solutions to these equations exist may be found by trial and error.

3.2. Comparison of optimal and robust control

Most of the robustness problems associated with \mathcal{H}_2 stem from the state estimation. Optimal controllers provided with full state information (i.e. without estimators) generally have excellent performance and robustness properties (Dailey *et al.* 1990). Note that the problems of control and state estimation in the \mathcal{H}_2 formulation $(\gamma \to \infty)$ are *decoupled*. Other than the system matrix \mathbf{A} , \mathbf{K} depends only upon $\{\ell, \mathbf{B}_2, \mathbf{C}_1\}$, and \mathbf{L} depends only upon $\{\alpha, \mathbf{B}_1, \mathbf{C}_2\}$. This is a result of the celebrated Separation Principle of the \mathcal{H}_2 formulation (Green & Limebeer 1995; Lewis & Syrmos 1995).

An important observation is that the problems of control and state estimation in the \mathscr{H}_{∞} formulation are coupled. Specifically, the computation of K in (3.6) depends on the expected covariance of the state disturbances, which are accounted for in B_1 , and the computation of L in (3.5) depends on the weightings in the cost function, which are accounted for in C_1 . This is one of the essential features of \mathscr{H}_{∞} control.

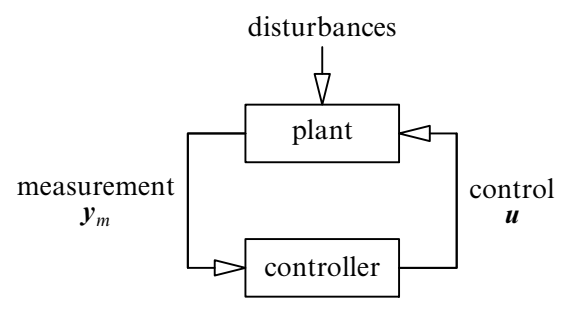
The \mathcal{H}_{∞} controller takes into account the expected covariance of the state disturbances, reflected in B_1 , when determining the state feedback matrix K. By so doing, the components of x that are expected to have the largest excitation by external disturbances are forced with the largest feedback by the relationship $u = K \hat{x}$ in the equation for the controller.

Similarly, the \mathcal{H}_{∞} estimator takes into account the weightings in the cost function, reflected in \mathbf{C}_1 , when determining the estimator feedback matrix \mathbf{L} . By so doing, the components of $\hat{\mathbf{x}}$ corresponding to the components of \mathbf{x} that are most important in the computation of the cost function are forced with the largest feedback by the relationship $\hat{\mathbf{u}} = \mathbf{L}(\mathbf{y} - \hat{\mathbf{y}})$ in the equation for the estimator.

By applying strong control only to those components of x significantly excited by external disturbances (by keeping ℓ large and reducing γ), and by applying strong estimator corrections only to those components of \hat{x} important in the computation of the cost function (by keeping α large and reducing γ), \mathscr{H}_{∞} feedback gains for components of the system not relevant to the control problem at hand may be kept at a minimum. With such feedback gains kept small, the stability properties of \mathscr{H}_{∞} estimator/controllers in the presence of system uncertainties may be dramatically improved over \mathscr{H}_2 counterparts which, for an equivalent worst-case response of the nominal plant, require reduced values of ℓ and α and, therefore, larger feedback gains. The reduced feedback applied in the \mathscr{H}_{∞} approach results in reduced opportunity for improper feedback to disrupt the closed-loop system.

3.3. Comparison with proportional control

A single-input, single-output (SISO) proportional controller for the present regulation problem is one which computes a single control variable simply by multiplying a single flow measurement by a complex scalar. In a slightly more general form, a multiple-input, multiple-output (MIMO) proportional controller computes each component of the control by a simple linear combination of multiple flow measurements, as shown in the following block diagram.



A proportional controller for the present problem takes the form $\mathbf{u} = \mathbf{K} \mathbf{y}_m$, where the (complex) elements of \mathbf{K} must be determined by parametric variation. It may be argued that the streamwise velocity fluctuations are more important than the spanwise velocity fluctuations in both case (i) and case (ii). Further, one can easily apply control at both walls based on local measurements of streamwise skin friction only. Thus, it is reasonable to consider two SISO proportional controllers for the present problem put together in a restricted MIMO form

$$\mathbf{u} = \begin{pmatrix} k_1 e^{i\phi_1} & 0 & 0 & 0 \\ 0 & k_2 e^{i\phi_2} & 0 & 0 \end{pmatrix} \mathbf{y}_m \equiv \mathbf{K} \mathbf{y}_m, \tag{3.7}$$

where the k_i and ϕ_i are chosen by parametric variation. It is found by such a parametric variation that $\phi_i = 0$ is most effective in this framework, and that the best performance is obtained near $k_1 = k_2 = 60$ for case (i) and $k_1 = k_2 = 10$ for case (ii). These restricted MIMO proportional controllers will be used as a basis for comparison in the analysis of the estimator/controllers based on modern control theory in § 6.

More general forms for K in a proportional controller may be considered, but, as the dimension of the problem grows, searching parametrically for effective K_{ij} becomes intractable, and the benefit of an approach based on control theory to determine the feedback matrices becomes apparent. With the present theory, the feedback matrices for systems of arbitrary dimension are developed as a function of just three scalar parameters $\{\gamma, \alpha, \ell\}$, each of which may be intuitively understood and individually adjusted to achieve desired system characteristics.

3.4. Numerical method

Standard numerical techniques are now applied to the control problem posed in (3.1)–(3.6). The algebraic Riccati equations are solved using the method of Laub (1991), which involves a Schur factorization. This is found to be a stable numerical algorithm for all cases tested. The implementation of Laub's method is written in Fortran 90 and follows closely the algorithm used by the Matlab function are.m (Grace et al. 1992). A Lyapunov solver, modelled after the Matlab function lyap.m, is also used. Two LAPACK routines (Anderson et al. 1995), zgeev.f and zgees.f, are used to compute eigenvalues/eigenvectors and Schur factorizations.

All routines are compiled in quad precision (128 bits per real number) to ensure sufficient numerical precision in the eigenvalue computation. Computations are carried out with N=140 for case (i) and N=70 for case (ii) to ensure good resolution of all significant eigenmodes. The eigenvalues of $\bf A$ for case (i) in table 1 match those tabulated by Orszag (1971) to eight significant figures, and the maximum transient energy growth for case (ii) in figure $\bf 3(b)$ matches that obtained by Butler & Farrell (1992) to four significant figures, indicating that the present numerical method is sufficiently accurate.

3.4.1. Spurious eigenmodes

It is a well-known computational challenge that, in addition to all of the well-resolved eigenmodes of a particular continuous PDE, several poorly resolved eigenmodes inevitably result from the solution of a discrete matrix eigenvalue problem. Such spurious eigenmodes are sometimes referred to as 'two-delta waves' because their dominant wavelength is approximately twice the local grid spacing. Unfortunately, the (spurious) eigenvalues of these poorly resolved eigenmodes may be near the (valid) eigenvalues of the well-resolved eigenmodes, even though the spurious modes are physically meaningless. For example, the first spurious eigenvalue computed for case (i) with N=140 occurs at $\lambda=-0.0235+1.520$ i. Spurious eigenmodes may be identified easily in two ways: (i) the eigenvalue λ moves significantly when N is modified slightly, though the remaining eigenvalues remain converged to all significant figures, and (ii) when plotted, spurious eigenvectors ξ are characterized by large oscillations from grid point to grid point across the domain, though converged eigenmodes are well resolved, as depicted in figure 1(b) in § 5.

Inclusion of spurious eigenmodes in the system matrix **A** to be controlled may cause problems when applying control theory to modify the closed-loop characteristics of the entire system, as these modes may be uncontrollable and/or unobservable. In order to ensure problems related to these modes do not arise, the spurious eigenmodes of **A** are identified, the corresponding eigenvalues modified to a 'benign', well-damped location, and the system matrix reconstructed according to

$$\mathbf{A}_{modified} = \mathbf{\Xi} \Lambda_{modified} \mathbf{\Psi}^*. \tag{3.8}$$

Note that $\Lambda_{modified}$ is the matrix of eigenvalues with the eigenvalues corresponding to spurious modes moved to $\lambda_{\kappa} = -500$, and Ψ and Ξ are the corresponding left and right eigenvector matrices. This ensures that the dynamics of these spurious modes are damped sufficiently to be insignificant with respect to the rest of the system. The modified matrix $\mathbf{A}_{modified}$ is implied by the symbol \mathbf{A} in the remainder of this work.

A minimal realization approach (Kailath 1980) is well suited to greatly reduce the dimension of the matrices and vectors involved, and thus the computer time needed, in the present computations. With this approach, uncontrollable, unobservable, spurious, and highly damped modes may be removed altogether from the representation of the system to be controlled. This idea will be explored in future work. The purpose of the present work, however, is to study the effects of control and estimation on the entire locus of eigenvalues in a well-resolved implementation. Thus, the matrix **A** is considered with no modifications beyond the damping of the spurious modes as described above. Note that, though controllers may be *designed* based on reduced systems, they must always be *analysed* based on the complete system to accurately characterize system behaviour.

4. Methods of analysis

This Section reviews four methods to analyse various properties of a generic system

$$\dot{\tilde{x}} = \tilde{\mathbf{A}}\,\tilde{x} + \tilde{\mathbf{B}}_1\,\tilde{w} + \tilde{\mathbf{B}}_2\,\tilde{\mathbf{u}},\tag{4.1a}$$

$$\tilde{z} = \tilde{\mathbf{C}}_1 \tilde{\mathbf{x}} + \tilde{\mathbf{D}}_{12} \tilde{\mathbf{u}}, \tag{4.1b}$$

$$\tilde{\mathbf{y}} = \tilde{\mathbf{C}}_2 \tilde{\mathbf{x}} + \tilde{\mathbf{D}}_{21} \tilde{\mathbf{w}}. \tag{4.1c}$$

The methods of analysis presented in this Section are applied to the present flow transition problem for the open-loop systems in § 5 and the closed-loop systems in § 6 by appropriate definition of the above tilde (~) variables in the respective sections. It is therefore instructive to first review the analysis techniques from a generic perspective.

In §4.1, the controllability and observability system Gramians are reviewed as a means to characterize the system as a whole. However, this approach alone does not characterize the stabilizability of uncontrollable systems or the detectability of unobservable systems. As shown in §4.2, it is useful to analyse the individual eigenmodes of the system under consideration separately, and to identify the degree to which each of these modes may be modified by the control and the sensitivity with which each may be detected by the observations. Non-orthogonality of the eigenmodes is reviewed in §4.3 as a method by which transient energy growth is possible in stable systems, and a method is discussed by which the maximum possible transient energy growth may be quantified. In §4.4, quantitative measures of the effects of both Gaussian and worst-case disturbances \tilde{w} on a relevant performance measure \tilde{z} are described. In § 4.5, it is shown that all four methods of analysis presented in this Section are immediately applicable to open-loop systems, closed-loop controllers with full state information, closed-loop estimators with no control, and composite closedloop estimator/controller systems by appropriate definition of the tilde (~) variables in (4.1).

4.1. System Gramians

We first address whether or not all of a given system's eigenmodes may be altered by the control \tilde{u} , and whether or not all of these eigenmodes may be discerned with the observations \tilde{y} . To accomplish this, it is standard practice (Lewis & Syrmos 1995) to consider two matrices which characterize the controllability and observability of the system (4.1) as a whole, assuming for the moment that $\tilde{w} = 0$. These are the system controllability Gramian L_c of (\tilde{A}, \tilde{B}_2) and the system observability Gramian L_o of (\tilde{C}_2, \tilde{A}) , which may be found by solution of

$$\tilde{\mathbf{A}} \mathbf{L}_c + \mathbf{L}_c \, \tilde{\mathbf{A}}^* + \tilde{\mathbf{B}}_2 \, \tilde{\mathbf{B}}_2^* = 0,$$

$$\tilde{\mathbf{A}}^* \mathbf{L}_o + \mathbf{L}_o \, \tilde{\mathbf{A}} + \tilde{\mathbf{C}}_2^* \, \tilde{\mathbf{C}}_2 = 0.$$

Stable numerical techniques to solve equations of this form, referred to as Lyapunov equations, are well developed (Bartels & Stewart 1972).

If L_c is (nearly) singular, there is at least one eigenmode of the system which is (nearly) unaffected by any choice of control \tilde{u} , and the system is called 'uncontrollable'. If all uncontrollable eigenmodes are stable, and the dynamics of the system may be made stable by the application of controller feedback, the system is called 'stabilizable'.

Similarly, if L_o is (nearly) singular, there is at least one eigenmode of the system which is (nearly) indiscernible by the observations \tilde{y} , and the system is called 'unobservable'. If all unobservable eigenmodes are stable, and the dynamics of the error of the estimate may be made stable by the application of estimator feedback, the system is called 'detectable'.

System Gramians alone do not identify which of the eigenmodes are unaffected by \tilde{u} or indiscernible by \tilde{y} . Thus, determination of whether or not an uncontrollable system is stabilizable or an unobservable system is detectable requires further analysis.

4.2. Eigenmode analysis

Modal canonical form (Kailath 1980) will now be used to quantify the sensitivity of each individual eigenmode of a system matrix $\tilde{\bf A}$ to both control and observation. Though this is common practice in linear systems theory (Skogestad & Postlethwaite 1996, pp. 122 and 126) a brief review helps establish two scalars, denoted here f_{κ} and g_{κ} , which indicate the controllability and observability of each individual eigenmode of the system.

Define the eigenvalues λ_{κ} and the left and right eigenvectors, ψ_{κ} and ξ_{κ} , and the corresponding eigenvalue and eigenvector matrices†, such that:

left eigenvectors: $\psi_{\kappa}^{*}\tilde{\mathbf{A}} = \lambda_{\kappa}\psi_{\kappa}^{*} \Rightarrow \Psi^{*}\tilde{\mathbf{A}} = \Lambda\Psi^{*},$ right eigenvectors: $\tilde{\mathbf{A}}\xi_{\kappa} = \lambda_{\kappa}\xi_{\kappa} \Rightarrow \tilde{\mathbf{A}}\Xi = \Xi\Lambda,$

where

$$oldsymbol{arLambda} = egin{pmatrix} \lambda_1 & & & & \\ & \lambda_2 & & \\ & & \ddots \end{pmatrix}, \quad oldsymbol{\Psi}^* = \left(rac{\pi}{N}
ight)^{1/2} egin{pmatrix} & oldsymbol{\psi}_1^* & & \\ & oldsymbol{\psi}_2^* & & \\ & draversign{pmatrix} & & & \\ & draversign{pmatrix} & & & \\ & & \ddots & & \\ & & & \ddots & \\ & & & \ddots$$

The system $\dot{\tilde{x}} = \tilde{A}\tilde{x}$ is stable if $\text{Re}(\lambda_{\kappa}) < 0$ for all κ . For systems (such as the present) with distinct eigenvalues, the (mutually orthogonal) left and right eigenvectors may be normalized such that

$$(\boldsymbol{\xi}_{\kappa}, \boldsymbol{\xi}_{\kappa}) = 1$$
 and $(\boldsymbol{\psi}_{\iota}, \boldsymbol{\xi}_{\kappa}) = \delta_{\iota \kappa} \Rightarrow \boldsymbol{\Psi}^* \boldsymbol{\Xi} = \boldsymbol{I}.$ (4.2)

Note that the right eigenvectors ξ_{κ} themselves are linearly independent but not orthogonal; i.e. $(\xi_{\iota}, \xi_{\kappa}) \neq 0$ for $\iota \neq \kappa$. Any \tilde{x} may be uniquely decomposed via a projection vector χ as a linear combination of these nonorthogonal right eigenvectors such that

$$\tilde{\mathbf{x}} = \mathbf{\Xi} \, \mathbf{\chi} = \sum_{\kappa} \chi_{\kappa} \, \boldsymbol{\xi}_{\kappa} \quad \Rightarrow \quad \dot{\tilde{\mathbf{x}}} = \mathbf{\Xi} \, \dot{\mathbf{\chi}} = \sum_{\kappa} \dot{\chi}_{\kappa} \, \boldsymbol{\xi}_{\kappa}. \tag{4.3}$$

4.2.1. Definition of modal control residual

By (4.1a) and (4.3) and assuming, for the moment, that $\tilde{w} = 0$, we have

$$\sum_{\kappa} \dot{\chi}_{\kappa} \, \boldsymbol{\xi}_{\kappa} = \tilde{\boldsymbol{A}} \sum_{\kappa} \chi_{\kappa} \, \boldsymbol{\xi}_{\kappa} + \tilde{\boldsymbol{B}}_{2} \, \tilde{\boldsymbol{u}} = \sum_{\kappa} \chi_{\kappa} \, \lambda_{\kappa} \, \boldsymbol{\xi}_{\kappa} + \tilde{\boldsymbol{B}}_{2} \, \tilde{\boldsymbol{u}}.$$

Taking the inner product with ψ_i

$$\left(\boldsymbol{\psi}_{\scriptscriptstyle I}, \sum_{\scriptscriptstyle K} \dot{\chi}_{\scriptscriptstyle K} \, \boldsymbol{\xi}_{\scriptscriptstyle K}\right) = \left(\boldsymbol{\psi}_{\scriptscriptstyle I}, \sum_{\scriptscriptstyle K} \chi_{\scriptscriptstyle K} \, \lambda_{\scriptscriptstyle K} \, \boldsymbol{\xi}_{\scriptscriptstyle K}\right) + \left(\boldsymbol{\psi}_{\scriptscriptstyle I}, \, \tilde{B}_{\scriptscriptstyle 2} \, \tilde{\boldsymbol{u}}\right)$$

and noting (2.10) and (4.2) yields

$$\dot{\chi}_{\kappa} = \lambda_{\kappa} \chi_{\kappa} + \frac{\pi}{N} (\tilde{\mathbf{B}}_{2}^{*} \boldsymbol{\psi}_{\kappa})^{*} \tilde{\boldsymbol{u}}.$$

If the vector $(\pi/N)\tilde{\boldsymbol{\beta}}_{2}^{*}\psi_{\kappa}=\mathbf{0}$, then $\dot{\chi}_{\kappa}=\lambda_{\kappa}\chi_{\kappa}$ for any $\tilde{\boldsymbol{u}}$. In other words, the component of $\tilde{\boldsymbol{x}}$ parallel to $\boldsymbol{\xi}_{\kappa}$ is not affected by the control $\tilde{\boldsymbol{u}}$, and the eigenmode is said to be

† The $(\pi/N)^{1/2}$ term in the definition of Ξ and Ψ is required to maintain consistency with the definition of an inner product which converges upon refining N, as discussed in § 2.4.

'uncontrollable'. Further, the 2-norm of the vector $(\pi/N)\tilde{\bf B}_2^*\psi_{\kappa}$,

$$f_{\kappa} = \frac{\pi}{N} \left(\boldsymbol{\psi}_{\kappa}^{*} \, \tilde{\boldsymbol{B}}_{2} \, \tilde{\boldsymbol{B}}_{2}^{*} \, \boldsymbol{\psi}_{\kappa} \right)^{1/2} \,, \tag{4.4}$$

termed here the 'control residual' of mode κ , is a quantitative measure of the sensitivity of the eigenmode κ to the control $\tilde{\boldsymbol{u}}$. Note the dependence of this expression on the matrix $\tilde{\boldsymbol{B}}_2 \tilde{\boldsymbol{B}}_2^*$, which is the matrix which drives the Lyapunov equation for controllability Gramian \boldsymbol{L}_c .

4.2.2. Definition of modal observation residual

By (4.1c) and (4.3) and assuming, for the moment, that $\tilde{\mathbf{w}} = \mathbf{0}$, we have

$$\tilde{\mathbf{y}} = \sum_{\kappa} \chi_{\kappa} \, \tilde{\mathbf{C}}_{2} \, \boldsymbol{\xi}_{\kappa}.$$

If the vector $\tilde{\mathbf{C}}_2 \boldsymbol{\xi}_{\kappa} = \mathbf{0}$, then $\tilde{\mathbf{y}}$ will not be a function of χ_{κ} . In other words, the component of $\tilde{\mathbf{x}}$ parallel to $\boldsymbol{\xi}_{\kappa}$ does not contribute to the observations $\tilde{\mathbf{y}}$, and the eigenmode is said to be 'unobservable'. Further, the (scaled) 2-norm of the vector $\tilde{\mathbf{C}}_2 \boldsymbol{\xi}_{\kappa}$,

$$g_{\kappa} = Re \left(\boldsymbol{\xi}_{\kappa}^{*} \, \tilde{\mathbf{C}}_{2}^{*} \, \tilde{\mathbf{C}}_{2} \, \boldsymbol{\xi}_{\kappa} \right)^{1/2}, \tag{4.5}$$

similarly termed the 'observation residual' of mode κ , is a quantitative measure of the sensitivity of the observation \tilde{y} to eigenmode κ . Note the dependence of this expression on the matrix $\tilde{\mathbf{C}}_{2}^{*}\tilde{\mathbf{C}}_{2}$, which is the matrix which drives the Lyapunov equation for observability Gramian \mathbf{L}_{o} . Note also that the scaling Re is used simply for numerical convenience.

4.3. Transient energy growth

Consider an initial state $\tilde{x}(0)$ of a stable system which may be decomposed into several constituent non-orthogonal eigenmodes which destructively interfere in such a way that the energy of the initial state $\mathscr{E}(0) = \tilde{x}^*(0) \, \mathbf{Q} \, \tilde{x}(0)$ is small. Such destructive interference may reduce in time as some eigenmodes decay more quickly than others. This can result in a large transient growth in the kinetic energy density $\mathscr{E}(t)$ of the state before an eventual exponential decay of energy at the rate of the least-stable constituent eigenmode.

Over a particular time interval τ , the shape of the most amplified initial conditions $\tilde{x}(0)$ may be found by a variational formulation (Butler & Farrell 1992). As introduced in (4.3), a state $\tilde{x}(0)$ may be decomposed onto the eigenvector matrix Ξ via a projection vector χ . Solving the system of simple ODEs resulting from application of (4.3) to (4.1a), assuming for the moment that $\tilde{u} = \tilde{w} = 0$, $\tilde{x}(t)$ may be written

$$\tilde{\mathbf{x}}(t) = \mathbf{\Xi} \, \mathrm{e}^{At} \, \mathbf{y},$$

where the projection χ is independent of time. The initial state $\tilde{x}(0)$ maximizing energy growth at $t = \tau$ may be found by considering the cost function

$$\begin{split} \mathscr{J}_{\mathscr{E}} &= \mathscr{E}(\tau) - \theta \left[\mathscr{E}(0) - 1 \right] \\ &= \tilde{\boldsymbol{x}}^*(\tau) \, \mathbf{Q} \, \tilde{\boldsymbol{x}}(\tau) - \theta \left[\tilde{\boldsymbol{x}}^*(0) \, \mathbf{Q} \, \tilde{\boldsymbol{x}}(0) - 1 \right] \\ &= \boldsymbol{\chi}^* \left(\mathbf{e}^{A^*\tau} \, \boldsymbol{\Xi}^* \, \mathbf{Q} \, \boldsymbol{\Xi} \, \mathbf{e}^{A\tau} \right) \boldsymbol{\chi} - \theta \left[\boldsymbol{\chi}^* \left(\boldsymbol{\Xi}^* \, \mathbf{Q} \, \boldsymbol{\Xi} \right) \boldsymbol{\chi} - 1 \right], \end{split}$$

setting the derivative with respect to the Lagrange multiplier θ equal to zero

$$\frac{\partial \mathcal{J}_{\mathscr{E}}}{\partial \theta} = 0 \quad \Rightarrow \quad \mathscr{E}(0) = 1$$

and the gradient with respect to the projection vector χ equal to zero

$$\frac{\partial \mathscr{J}_{\mathscr{E}}}{\partial \chi} = 0 \quad \Rightarrow \quad (e^{A^*\tau} \, \mathbf{\Xi}^* \, \mathbf{Q} \, \mathbf{\Xi} \, e^{A\tau}) \, \chi = \theta \, (\mathbf{\Xi}^* \, \mathbf{Q} \, \mathbf{\Xi}) \, \chi$$

$$\Rightarrow \quad \theta = \frac{\mathscr{E}(\tau)}{\mathscr{E}(0)} = \frac{\chi^* \, (e^{A^*\tau} \, \mathbf{\Xi}^* \, \mathbf{Q} \, \mathbf{\Xi} \, e^{A\tau}) \, \chi}{\chi^* \, (\mathbf{\Xi}^* \, \mathbf{Q} \, \mathbf{\Xi}) \, \chi}.$$

The first condition normalizes the energy of the initial state. The second condition results in a generalized eigenproblem of the form $\mathbf{R} \chi = \theta \mathbf{S} \chi$, whose maximum eigenvalue θ_{max} corresponds to the maximum energy growth $\mathcal{E}(\tau)/\mathcal{E}(0)$ by the corresponding initial state $\tilde{\mathbf{x}}(0) = \mathbf{\Xi} \chi_{max}$. A search routine may be used to find the time interval τ for which this approach leads to the greatest possible energy growth.

4.4. Transfer function norms

Quantitative measures of the effects of both Gaussian and worst-case disturbances \tilde{w} on relevant performance measures \tilde{z} are sought to characterize the various systems. The 2-norm and the ∞ -norm of the transfer function from \tilde{w} to \tilde{z} , which we shall call here $T_{\tilde{z}\tilde{w}}$, are commonly used for this purpose.

Taking the Laplace transform of the generic system (4.1), assuming for the moment that $\tilde{u} = 0$, it is easy to determine the transfer function $T_{\tilde{z}\tilde{w}}(s)$ from $\tilde{w}(s)$ to $\tilde{z}(s)$ (the Laplace transforms of \tilde{w} and \tilde{z}) such that

$$\tilde{z}(s) = \tilde{\mathbf{C}}_1 (s \mathbf{I} - \tilde{\mathbf{A}})^{-1} \tilde{\mathbf{B}}_1 \tilde{\mathbf{w}}(s) \equiv \mathbf{T}_{\tilde{z}\tilde{\mathbf{w}}}(s) \tilde{\mathbf{w}}(s).$$

Norms the transfer function $T_{\tilde{z}\tilde{w}}(s)$, also referred to as system norms, quantify how relevant performance measures \tilde{z} respond to disturbances \tilde{w} in the present systems, as shown below. These norms turn out to be finite for all \mathcal{H}_2 - and \mathcal{H}_{∞} -controlled systems considered here, but not for the proportionally controlled systems, as explained in detail in § 4.6.

4.4.1. Transfer function 2-norms

The 2-norm of a stable transfer function $T_{\tilde{z}\tilde{w}}(s)$ may be defined (Doyle *et al.* 1989) as

$$||\mathbf{T}_{\tilde{z}\tilde{w}}||_{2}^{2} \equiv \frac{1}{2\pi} \int_{-\infty}^{\infty} \operatorname{trace}\left[\mathbf{T}_{\tilde{z}\tilde{w}}(j\omega)^{*}\mathbf{T}_{\tilde{z}\tilde{w}}(j\omega)\right] d\omega. \tag{4.6}$$

It is finite when $\tilde{\mathbf{A}}$ is stable (i.e. all of the eigenvalues of $\tilde{\mathbf{A}}$ have negative real part) and $\mathbf{T}_{\tilde{z}\tilde{w}}(j\omega)$ is 'strictly proper' (i.e. when $\mathbf{T}_{\tilde{z}\tilde{w}}(j\omega) \to \mathbf{0}$ as $\omega \to \infty$).

The norm $||\mathbf{T}_{\tilde{z}\tilde{w}}||_2$ is a very useful measure, as it is exactly the expected r.m.s. value of the output \tilde{z} , i.e. $||\mathbf{T}_{\tilde{z}\tilde{w}}||_2^2 = E[\tilde{z}^*\tilde{z}]$, when the input \tilde{w} is a unit variance white Gaussian process. The 2-norm of $\mathbf{T}_{\tilde{z}\tilde{w}}$ may be found by solving a Lyapunov equation

$$\tilde{\mathbf{A}}^* \mathbf{L}_o + \mathbf{L}_o \tilde{\mathbf{A}} + \tilde{\mathbf{C}}_1^* \tilde{\mathbf{C}}_1 = \mathbf{0} \quad \Rightarrow \quad ||\mathbf{T}_{\tilde{z}\tilde{w}}||_2^2 = \operatorname{trace}(\tilde{\mathbf{B}}_1^* \mathbf{L}_o \tilde{\mathbf{B}}_1).$$

As stated previously, stable numerical techniques to solve Lyapunov equations are well developed (Bartels & Stewart 1972).

4.4.2. Transfer function ∞-norms

The ∞ -norm of a stable transfer function $T_{\tilde{z}\tilde{w}}$ may be defined (Doyle et al. 1989) as

$$||\mathbf{T}_{\tilde{z}\tilde{w}}||_{\infty} \equiv \sup_{\omega} \sigma_{max} \left[\mathbf{T}_{\tilde{z}\tilde{w}}(j\omega) \right] \quad \text{with} \quad \sigma_{max} \equiv \text{maximum singular value.}$$
 (4.7)

It is finite when $\tilde{\mathbf{A}}$ is stable (i.e. all of the eigenvalues of $\tilde{\mathbf{A}}$ have negative real part) and $\mathbf{T}_{\tilde{z}\tilde{w}}(j\omega)$ is 'semi-proper' (i.e. when $\mathbf{T}_{\tilde{z}\tilde{w}}(j\omega)$ is finite as $\omega \to \infty$).

The norm $||T_{\tilde{z}\tilde{w}}||_{\infty}$ is very useful, as it is a measure of the 'worst case' amplification of the disturbance \tilde{w} by the system. Unfortunately, the ∞ -norm of $T_{\tilde{z}\tilde{w}}$ must be sought by an iterative search. The approach used here, suggested by Doyle *et al.* (1989), is

- (a) guess a value of γ ;
- (b) compute the eigenvalues of the Hamiltonian $\mathbf{H} = \begin{pmatrix} \tilde{\mathbf{A}} & \frac{1}{\gamma^2} \tilde{\mathbf{B}}_1 \tilde{\mathbf{B}}_1^* \\ -\tilde{\mathbf{C}}_1^* \tilde{\mathbf{C}}_1 & -\tilde{\mathbf{A}}^* \end{pmatrix}$,
- (c) $||\mathbf{T}_{\tilde{z}\tilde{w}}||_{\infty} < \gamma$ iff \mathbf{H} has no eigenvalues on the imaginary axis and $\mathbf{H} \in \text{dom}(\text{Ric})$. (See Doyle *et al.* 1989 for definition of the latter property.) Thus, we may increase or decrease γ accordingly, using a golden section search, and repeat from (b) until bounds on $||\mathbf{T}_{\tilde{z}\tilde{w}}||_{\infty}$ reach a desired tolerance.

4.4.3. Performance measures \tilde{z} to be considered

For the characterization of the present closed-loop systems, two separate performance measure \tilde{z} will be considered. The first performance measure \tilde{z}_1 , obtained by setting $C_1 = Q^{1/2}$ and $D_{12} = 0$ (and thus $\tilde{z}_1^* \tilde{z}_1 = x^* Q x$), allows us to evaluate the norms of the transfer function from the disturbance w to the energy of the state x. For notational convenience, the transfer function from the disturbance w to the performance measure \tilde{z}_1 is denoted T_{xw} in the remainder of this work.

The second performance measure \tilde{z}_2 , obtained by setting $C_1 = 0$ and $D_{12} = I$ (and thus $\tilde{z}_2^* \tilde{z}_2 = u^* u$), allows us to evaluate the norms of the transfer function from the disturbance w to the control u. For notational convenience, the transfer function from the disturbance w to the performance measure \tilde{z}_2 is denoted T_{uw} in the remainder of this work. Note that, since $z^* z = x^* Q x + \ell^2 u^* u$ by (3.4), it follows that the 2-norm of the transfer function from the disturbance to the performance measure z actually used in the computation of the controller is just

$$||\mathbf{T}_{zw}||_2^2 = ||\mathbf{T}_{xw}||_2^2 + \ell^2 ||\mathbf{T}_{uw}||_2^2. \tag{4.8}$$

4.5. Systems to be analysed

Four systems are now described and algebraically manipulated into the generic system form (4.1) presented at the beginning of this Section. By so doing, any of the analysis techniques described above may be readily applied to any of the systems described below simply by appropriate definition of the tilde (~) variables in (4.1). This versatile analysis approach is exploited in subsequent Sections to characterize the open-loop and closed-loop systems, and is a significant design advantage of modern control theory.

System 1. Open-loop plant ((3.1) with (3.4b):

$$\begin{vmatrix}
 \dot{x} = A & x + B_1 & w + B_2 & u, \\
 z = C_1 x & + D_{12} u, \\
 y = C_2 x + D_{21} w.
 \end{vmatrix}$$
(4.9)

System 2. Closed-loop plant with controller and full state information ((3.1) with (3.4b) and (3.3) augmented with extra control feedback term u', assuming $\hat{x} = x$):

Plant:
$$\begin{cases} \dot{x} = \mathbf{A} \ x + \mathbf{B}_1 \mathbf{w} + \mathbf{B}_2 \ \mathbf{u}, \\ z = \mathbf{C}_1 x + \mathbf{D}_{12} \mathbf{u}, \end{cases}$$
Controller:
$$\begin{cases} \mathbf{u} = \mathbf{K} \ x + \mathbf{u}'. \end{cases}$$

Simple algebraic manipulation yields the generic form for analysis:

$$\begin{vmatrix}
\dot{x} = (\mathbf{A} + \mathbf{B}_2 \mathbf{K}) & x + \mathbf{B}_1 \mathbf{w} + \mathbf{B}_2 \mathbf{u}', \\
z = (\mathbf{C}_1 + \mathbf{D}_{12} \mathbf{K}) x & + \mathbf{D}_{12} \mathbf{u}', \\
y \equiv x.
\end{vmatrix} (4.10)$$

System 3. Closed-loop plant with estimator and no control ((3.1) and (3.2) augmented with extra estimator feedback term \hat{u}' , assuming u = 0):

Plant:
$$\begin{cases} \dot{x} = \mathbf{A} \ x + \mathbf{B}_1 \ w, \\ y = \mathbf{C}_2 x + \mathbf{D}_{21} w, \end{cases}$$
Estimator:
$$\begin{cases} \dot{\hat{x}} = \mathbf{A} \ \hat{x} - \hat{u}, \\ \hat{y} = \mathbf{C}_2 \ \hat{x}, \\ \hat{u} = \mathbf{L} \ (y - \hat{y}) + \hat{u}'. \end{cases}$$

Defining x_E as the state estimation error $x_E \equiv x - \hat{x}$ and and y_E as the measurement error $y_E \equiv y - \hat{y}$, simple algebraic manipulation yields the generic form for analysis:

$$\begin{aligned}
\dot{\mathbf{x}}_{E} &= (\mathbf{A} + \mathbf{L}\mathbf{C}_{2}) \, \mathbf{x}_{E} + (\mathbf{B}_{1} + \mathbf{L}\mathbf{D}_{21}) \, \mathbf{w} + \hat{\mathbf{u}}', \\
\mathbf{z}_{E} &\equiv \mathbf{C}_{1} \quad \mathbf{x}_{E}, \\
\mathbf{y}_{E} &= \mathbf{C}_{2} \quad \mathbf{x}_{E} + \mathbf{D}_{21} \quad \mathbf{w}.
\end{aligned} \tag{4.11}$$

System 4. Closed-loop plant with estimator and controller ((3.1) with (3.4b), (3.2) and (3.3) augmented with extra control feedback term u':

Plant:
$$\begin{cases} \dot{x} = \mathbf{A} \ x + \mathbf{B}_1 \mathbf{w} + \mathbf{B}_2 \mathbf{u}, \\ z = \mathbf{C}_1 x + \mathbf{D}_{12} \mathbf{u}, \\ y = \mathbf{C}_2 x + \mathbf{D}_{21} \mathbf{w}, \end{cases}$$
Estimator:
$$\begin{cases} \dot{x} = \mathbf{A} \ \hat{x} - \hat{\mathbf{u}} + \mathbf{B}_2 \mathbf{u}, \\ \hat{y} = \mathbf{C}_2 \hat{x}, \\ \hat{u} = \mathbf{L} \ (y - \hat{y}), \end{cases}$$
Controller:
$$\{ \mathbf{u} = \mathbf{K} \ \hat{x} + \mathbf{u}'. \end{cases}$$

Optimal and robust control and estimation of linear paths to transition

Simple algebraic manipulation yields the generic form for analysis:

$$\begin{pmatrix}
\dot{x} \\
\dot{x}_{E}
\end{pmatrix} = \begin{pmatrix}
\mathbf{A} + \mathbf{B}_{2}\mathbf{K} & -\mathbf{B}_{2}\mathbf{K} \\
0 & \mathbf{A} + \mathbf{L}\mathbf{C}_{2}
\end{pmatrix} \begin{pmatrix}
x \\
x_{E}
\end{pmatrix} + \begin{pmatrix}
\mathbf{B}_{1} \\
\mathbf{B}_{1} + \mathbf{L}\mathbf{D}_{21}
\end{pmatrix} \mathbf{w} + \begin{pmatrix}
\mathbf{B}_{2} \\
0
\end{pmatrix} \mathbf{u}',$$

$$z = (\mathbf{C}_{1} + \mathbf{D}_{12}\mathbf{K} - \mathbf{D}_{12}\mathbf{K}) \begin{pmatrix}
x \\
x_{E}
\end{pmatrix} + \mathbf{D}_{12}\mathbf{u}',$$

$$y_{E} = \begin{pmatrix}
0 & \mathbf{C}_{2}
\end{pmatrix} \begin{pmatrix}
x \\
x_{E}
\end{pmatrix} + \mathbf{D}_{21}\mathbf{w}.$$
(4.12)

4.6. Analysis of semi-proper proportionally controlled systems

When a proportional controller, such as that proposed in §3.3, is applied to the present problem, the resulting system may be written in the form

$$\dot{x} = \mathbf{A} x + \mathbf{B}_1 w + \mathbf{B}_2 u, \tag{4.13}$$

$$z = \mathbf{C}_1 x + \mathbf{D}_{12} \mathbf{u}, \tag{4.14}$$

$$z = C_1 x + D_{12} u,$$
 (4.14)
 $y_m = C_2 x + D_{21} w + D_{22} u,$ (4.15)

$$\mathbf{u} = \mathbf{K} \, \mathbf{y}_m, \tag{4.16}$$

with **K** of a simple form, such as that in (3.7). Combining to eliminate u and y_m gives

$$\dot{x} = [\mathbf{A} + \mathbf{B}_2 (\mathbf{I} - \mathbf{K} \mathbf{D}_{22})^{-1} \mathbf{K} \mathbf{C}_2] x + [\mathbf{B}_1 + \mathbf{B}_2 (\mathbf{I} - \mathbf{K} \mathbf{D}_{22})^{-1} \mathbf{K} \mathbf{D}_{21}] w,$$

$$z = [\mathbf{C}_1 + \mathbf{D}_{12} (\mathbf{I} - \mathbf{K} \mathbf{D}_{22})^{-1} \mathbf{K} \mathbf{C}_2] x + [\mathbf{D}_{12} (\mathbf{I} - \mathbf{K} \mathbf{D}_{22})^{-1} \mathbf{K} \mathbf{D}_{21}] w,$$

which we may write more simply as

$$\dot{x} \equiv \tilde{\mathbf{A}} x + \tilde{\mathbf{B}}_1 w,$$
 $z \equiv \tilde{\mathbf{C}}_1 x + \tilde{\mathbf{D}}_{11} w.$

The eigenvalues and eigenvectors of $\tilde{\bf A}$ may be examined to characterize the behaviour of the closed-loop system in the absence of disturbances w and quantify the maximum transient energy growth using the techniques of §4.2 and §4.3.

Given this type of control, the transfer function from w(s) to z(s) is now

$$z(s) = [\tilde{\mathbf{C}}_1 (s \mathbf{I} - \tilde{\mathbf{A}})^{-1} \tilde{\mathbf{B}}_1 + \tilde{\mathbf{D}}_{11}] w(s) \equiv \mathbf{T}_{zw}(s) w(s).$$

Setting $C_1 = Q^{1/2}$ and $D_{12} = 0$, and thus $z^* z = x^* Q x$ (our first performance measure), the norms of the transfer function from the disturbance w to the energy of the state x, $||T_{xw}||_2$ and $||T_{xw}||_{\infty}$, can be evaluated using the techniques of §4.4. Note that, in this case, $\tilde{\mathbf{D}}_{11} = \mathbf{0}$.

Setting $C_1 = 0$ and $D_{12} = I$, and thus $z^*z = u^*u$ (our second performance measure), we see that the transfer function from the disturbance w to the control u is not 'strictly proper' (Skogestad & Postlethwaite 1996, p. 5), as there is a direct feedthrough term from the disturbance w to the control u; in this case, $\tilde{\mathbf{D}}_{11} \neq \mathbf{0}$. As there is a term of $T_{uw}(s)$ which is constant for all s, the system is termed 'semi-proper', and thus, by its definition in (4.6), it is clear that $||\mathbf{T}_{uw}||_2 = \infty$.

The main point here is that a controller with a proportional component, such as the PI controller proposed by Joshi et al. (1997), will not have built-in high-frequency roll-off of the controller response, and measurement noise will feed directly through to the controller input. Thus, the r.m.s. value of the control u in response to a unit variance white Gaussian disturbance w is infinite. In practice, limitations in the response of the actuators and the controlling electronics would limit the r.m.s. response of a proportional controller to white-noise disturbances. An ad hoc low-pass filter is required to achieve high-frequency roll-off of the proportional component of a PI controller below those frequencies set by the implementation hardware itself. An advantage of the optimal and robust approaches developed in this paper is that the resulting systems are strictly proper, and thus an appropriate amount of high-frequency roll-off is built-in as a natural result of the control formulation (i.e. $T_{zw}(j\omega) \to 0$ appropriately quickly as $\omega \to \infty$). Simulations of the idealized optimal and robust closed-loop systems developed in this article can be used to determine what high-frequency performance of the implementation hardware is necessary for the desired performance of a given system.

5. Analysis of uncontrolled, open-loop system

The uncontrolled ('open-loop') system is now examined in detail using the methods of analysis of §4 by consideration of system 1 in §4.5.

5.1. System Gramians

For both case (i) and case (ii) of the present system, the smallest eigenvalues of both system Gramians, \mathbf{L}_c and \mathbf{L}_o , are computed to be near machine zero, indicating that these systems are both uncontrollable and unobservable. To obtain information on stabilizability and detectability, analysis of the individual eigenmodes is necessary.

5.2. Eigenmode analysis

5.2.1. Eigenmode analysis of case (i)

The least-stable eigenvalues of **A** for case (i) are plotted in figure 1(a) and tabulated, along with the corresponding control and observation residuals f_{κ} and g_{κ} , in table 1. Figure 1(b) shows the shape of the eigenvectors corresponding to the six least-stable eigenvalues along with an example of a spurious mode as discussed in § 3.4.1.

An important observation from figure 1(b) is that eigenvalues in the upper branch of figure 1(a) have corresponding eigenvectors with variations primarily in the centre of the channel, and thus it may be expected that these modes will be less controllable via wall transpiration and less observable via wall measurements than eigenmodes in the lower branch. This observation is quantified by smaller values of f_{κ} and g_{κ} for these modes.

Note from table 1 that the third eigenmode is five orders of magnitude less sensitive than the first eigenmode to modifications in the control. In general, those modes in the upper branch of figure 1(a) (large $|\text{Im}(\lambda)|$) are much less sensitive to control than those in the lower branch (small $|\text{Im}(\lambda)|$). Near the intersection of the two branches (Re(λ) ≈ -0.3), the control residual is maximum, while it decreases slowly to the left of this intersection (Re(λ) < -0.3). It can be predicted that the closed-loop eigenmodes corresponding to the largest f_{κ} might be affected most upon application of controller feedback. Indeed, Joshi *et al.* (1997) report difficulty with the destabilization of mode $\kappa = 37$, the mode with the largest f_{κ} , by application of their PI controller.

Note also from table 1 that the flow measurements are two orders of magnitude less sensitive to the third eigenmode than they are to the first eigenmode. It can be predicted that the closed-loop eigenmodes corresponding to the largest g_{κ} might be affected most upon application of estimator feedback.

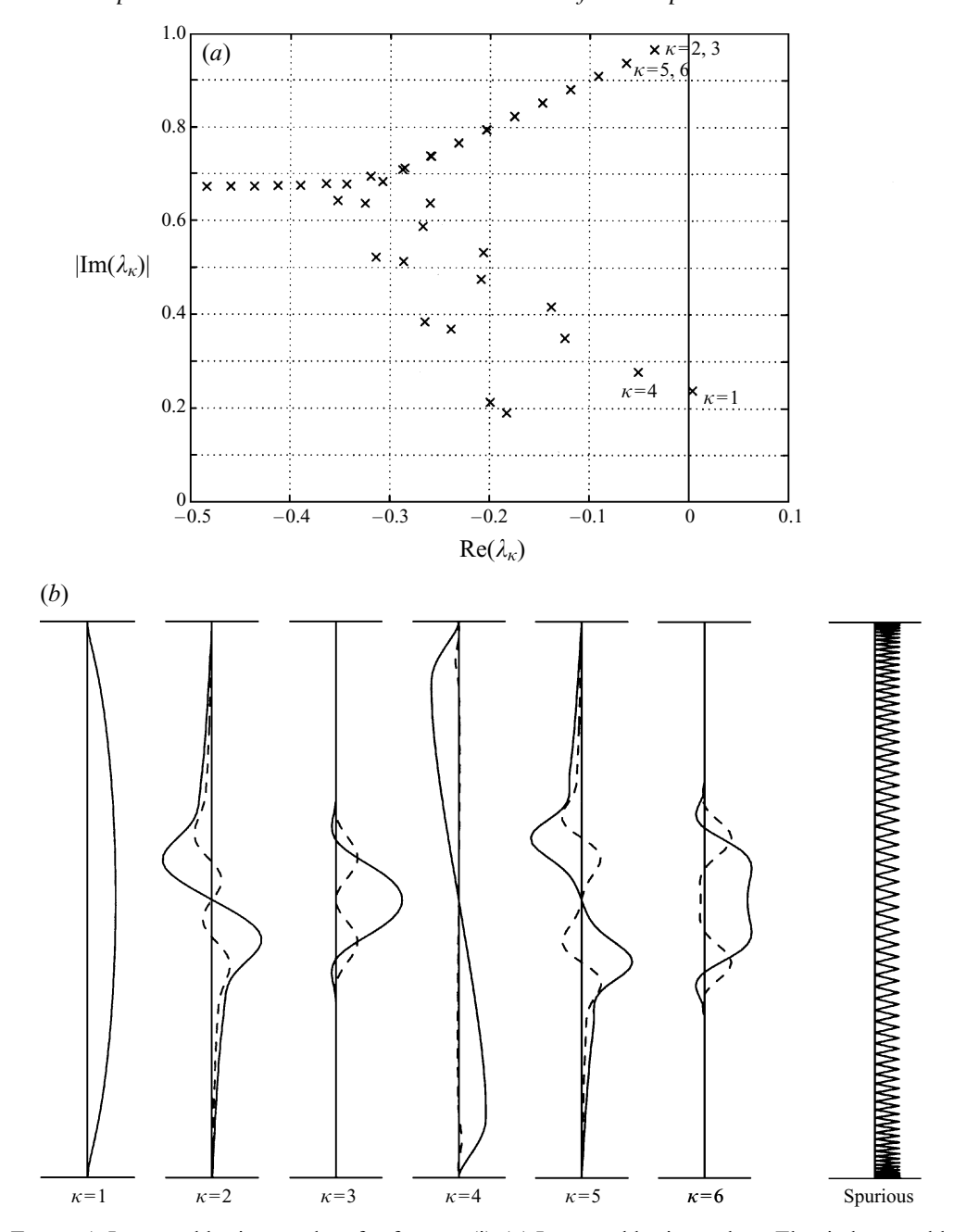


FIGURE 1. Least-stable eigenmodes of **A** for case (i). (a) Least-stable eigenvalues. The six least-stable eigenmodes are labelled. (b) Real (solid) and imaginary (dashed) parts of the v component of the eigenvectors corresponding to the six eigenvalues labelled in (a) and the spurious, unresolved eigenmode discussed in § 3.4.1 (initially located at $\lambda = -0.0214 + 1.514i$ and later damped to remove its influence), plotted as a function of y from the lower wall (bottom) to the upper wall (top). The corresponding ω components of these eigenvectors are zero.

κ	λ_{κ}	f_{κ}	g_{κ}
1	0.00373967 - 0.23752649 i	0.266545	102.61
2	-0.03516728 - 0.96463092i	0.000215	72.85
3	-0.03518658 - 0.96464251 i	0.000005	1.45
4	-0.05089873 - 0.27720434i	0.026606	347.98
5	-0.06320150 - 0.93631654i	0.000513	81.39
6	-0.06325157 - 0.93635178i	0.000021	2.90
7	-0.09122274 - 0.90798305 i	0.000931	83.36
8	-0.09131286 - 0.90805633 i	0.000056	4.32
9	-0.11923285 - 0.87962729 i	0.001587	77.67
10	-0.11937073 - 0.87975570i	0.000124	5.37
11	-0.12450198 - 0.34910682i	0.171859	69.50
12	-0.13822653 - 0.41635102i	0.037660	252.09
13	-0.14723393 - 0.85124584i	0.002833	63.31
14	-0.14742560 - 0.85144938 i	0.000268	5.59
15	-0.17522868 - 0.82283504i	0.005581	44.14
:	÷	:	:
37	-0.32519719 - 0.63610486i	5.659801	0.78
38	-0.34373267 - 0.67764346 i	4.685315	0.64
:	:	:	:
52	-0.66286552 - 0.67027520 i	0.259581	11.58
:	<u>:</u>	:	:

Table 1. Least-stable eigenmodes of **A** for case (i) and the associated control and observation residuals. Calculation used Chebyshev collocation technique with N=140 in quad precision. The only unstable mode ($\kappa=1$) is both sensitive to the control u and easily detected by the observations y.

5.2.2. Eigenmode analysis of case (ii)

The least-stable eigenvalues of **A** for case (ii) are plotted in figure 2(a) and tabulated, along with the corresponding control and observation residuals f_{κ} and g_{κ} , in table 2. Figure 2(b) shows the shape of the eigenvectors corresponding to the nine least-stable eigenvalues. Note that all eigenmodes shown span the entire channel, and thus f_{κ} and g_{κ} are all O(1); i.e. the least-stable eigenmodes are both observable and controllable.

An important observation from figure 2 is that the eigenvalues in this case tend to come in nearly identical pairs, and the corresponding eigenvectors are nearly parallel. This structure may be explained by examination of the governing equations. Defining $\Delta_v \equiv \mathscr{D} \widetilde{\mathscr{D}} - k_z^2 I$ and $\Delta_\omega \equiv \mathscr{D} \mathscr{D} - k_z^2 I$, the discrete form of (2.4) when $k_x = 0$ is

$$\begin{array}{lll} \varDelta_{v}\,\dot{\boldsymbol{v}} = \left\{\varDelta_{v}(\varDelta_{v}/Re)\right\}\,\boldsymbol{v} \\ \dot{\boldsymbol{\omega}} \ = \left\{-\mathrm{i}\,k_{z}\,U'\right\} & \boldsymbol{v} \ + \left\{\varDelta_{\omega}/Re\right\}\,\boldsymbol{\omega}. \end{array} \Rightarrow \begin{array}{ll} \dot{\boldsymbol{v}} = \mathscr{L}\,\boldsymbol{v} \\ \dot{\boldsymbol{\omega}} = \mathscr{C}\,\boldsymbol{v} \ + \mathscr{S}\,\boldsymbol{\omega} \end{array} \Rightarrow \dot{\boldsymbol{x}} = \boldsymbol{A}\boldsymbol{x} + \boldsymbol{B}\boldsymbol{u}, \end{array}$$

where $\mathscr{L} = \Delta_v/Re$, $\mathscr{C} = -\mathrm{i}\,k_z\,U'I$, and $\mathscr{S} = \Delta_\omega/Re$, and \mathscr{L}_c , \mathscr{C}_c , and \mathscr{S}_c are the centre blocks of \mathscr{L} , \mathscr{C} , and \mathscr{S} respectively, as discussed in §2.2. Note that the only difference between \mathscr{S} and \mathscr{L} is the treatment of boundary conditions in the derivative operators of Δ_v and Δ_ω . The eigenvalues of the system matrix \mathbf{A} are the union of the eigenvalues of \mathscr{S}_c and the eigenvalues of \mathscr{L}_c . Due to the similarity of these two matrices when $k_x = 0$, the eigenvalues of \mathbf{A} tend to come in nearly identical pairs, as shown in figure 2(a).

Note that half of the eigenvectors of $\mathbf{A} \mathbf{x} = \lambda \mathbf{x}$ correspond to the eigenvectors of

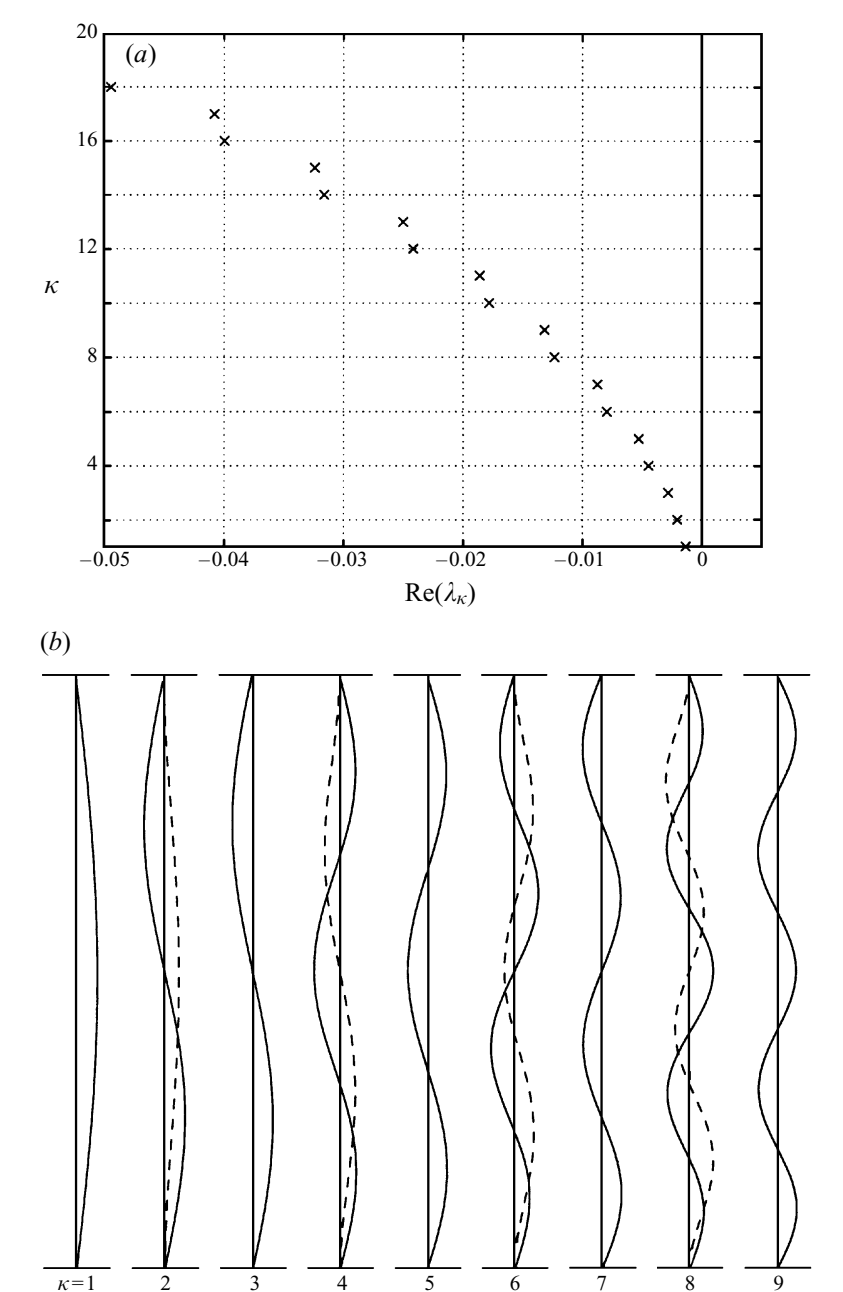


FIGURE 2. Least-stable eigenmodes of **A** for case (ii). (a) Least-stable eigenvalues. Imaginary components of all eigenvalues are negligible. (b) Real part of the ω component of the eigenvectors (solid) and 1000 times the imaginary part of the v component of the eigenvectors (dashed) corresponding to the least-stable eigenvalues of (a), plotted as a function of v from the lower wall (bottom) to the upper wall (top). Imaginary part of the v components and real part of the v components of these eigenvectors are negligible.

κ	λ_{κ}	f_{κ}	g_{κ}
1	-0.00132907	0.9619	1.0396
2	-0.00205172	0.9932	1.8656
3	-0.00280951	0.5092	1.9641
4	-0.00444971	1.0457	2.3710
5	-0.00527691	0.3478	2.8749
6	-0.00794734	0.9150	2.9317
7	-0.00873127	0.2646	3.7789
8	-0.01233325	0.8009	3.5058
9	-0.01317259	0.2137	4.6786
10	-0.01781312	0.6841	4.1763
11	-0.01860088	0.1794	5.5751
:	:	:	:
	•	•	

Table 2. Least-stable eigenmodes of \boldsymbol{A} for case (ii) and the associated control and observation residuals. Calculation used Chebyshev collocation technique with N=70 in quad precision. All modes are stable and all eigenvalues real.

 $\mathscr{S}\omega = \lambda \omega$ with $\mathbf{v} = \mathbf{0}$. The other half of the eigenvectors of \mathbf{A} correspond to the eigenvectors of $\mathscr{L}\mathbf{v} = \lambda \mathbf{v}$ with $\omega = -(\mathscr{L} - \lambda \mathbf{I})^{-1}\mathscr{C}\mathbf{v}$. Since the matrix $(\mathscr{L} - \lambda \mathbf{I})$ is nearly singular, $||\mathbf{v}||/||\omega|| \ll 1$ in this second set of eigenvectors. Further, as the eigenvalues of the second set are near those of the first set, the (dominant) ω components of the two sets of eigenvectors are nearly parallel, as shown in figure 2(b).

5.3. Transient energy growth

The exponential energy growth possible in case (i), as shown in figure 3(a), is well predicted by examining the eigenvalues for this case in figure 1(a), as a system eigenvalue in the right half-plane implies an unstable mode. The eigenvalues move to the left half-plane as stabilizing estimators and controllers are applied to the system.

The large but finite transient energy growth possible in case (ii), which reaches a maximum of $\mathcal{E}(\tau)/\mathcal{E}(0) = 4897$ for the uncontrolled system as shown in figure 3(b), can not be predicted by examination of the eigenvalues for this case in figure 2(a). Such a large transient energy growth in a linearly stable system is possible because the eigenvectors of case (ii) are highly non-orthogonal, as shown in figure 2(b). The mechanism for this large energy growth is explained in physical terms in figure 4. For small but finite initial flow perturbations, O(Re) transient energy growth may be large enough to stimulate nonlinear instabilities in the flow and instigate transition to turbulence. In § 6.4, the maximum transient energy growth for case (ii), $\max_{\tau,x(0)} \{\mathcal{E}(\tau)/\mathcal{E}(0)\}$, is shown to be significantly reduced as estimators and controllers are applied to the system.

5.4. Transfer function norms

As described in §4.4, in order to quantify the behaviour of the state response to disturbances and the control response to disturbances separately, norms of the transfer functions T_{xw} and T_{uw} will be computed separately. Three norms will be considered: $||T_{xw}||_2$ is a measure of the state response to Gaussian disturbances, $||T_{xw}||_{\infty}$ is a measure of the state response to worst-case disturbances, and $||T_{uw}||_2$ is a measure of the control used in response to Gaussian disturbances. These transfer function norms will be used as benchmarks in §6.1 to quantify the effects of control and estimation for the present systems.

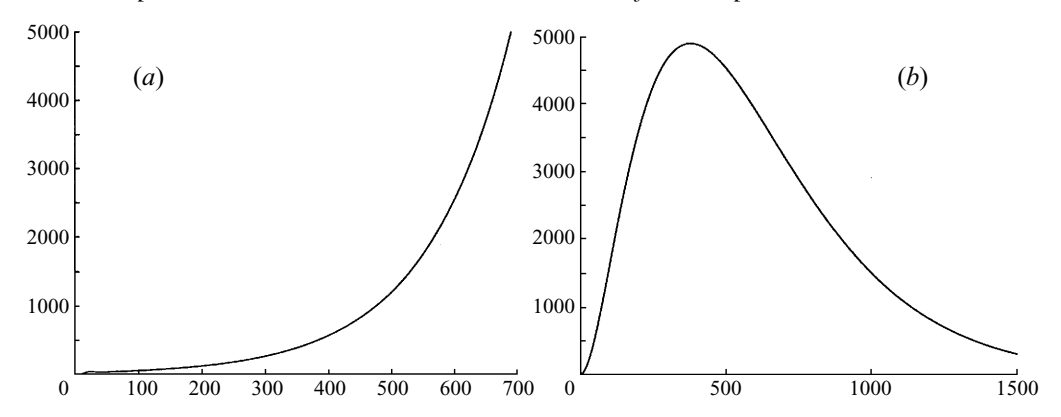


FIGURE 3. Maximum energy growth for open-loop, uncontrolled systems: $\mathcal{E}(t)/\mathcal{E}(0)$ versus t. (a) Case (i), unstable. (b) Case (ii), stable. Transient energy growth at $\tau = 379$ is $\mathcal{E}(\tau)/\mathcal{E}(0) = 4897$.

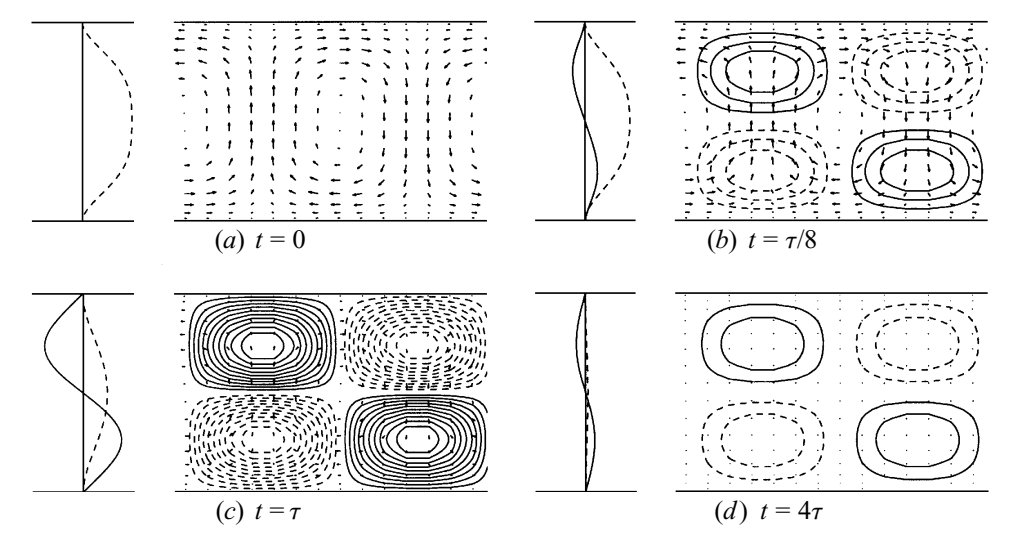


FIGURE 4. Shape of the flow perturbation with the largest transient energy growth for case (ii), as plotted in figure 3(b). At the left of each subfigure is the perturbation plotted as in figure 2(b), with the v component (dashed) magnified by a factor of 250 as compared with the ω component (solid). The corresponding flow perturbation in a cross-flow plane is shown at the right of each subfigure, with the cross-flow velocity vectors shown as arrows and the streamwise velocity as contours; recall that the flow perturbations for case (ii), with $k_x = 0$, have no streamwise variation. The initial perturbation (a superposition of several eigenmodes) is a streamwise vortex filling the channel with zero streamwise velocity component. The streamwise vorticity diminishes with time, during which very large streamwise velocity fluctuations are induced by its action on the mean streamwise velocity profile U(y). Positive streamwise velocity regions ('sweeps') are indicated with solid contours, and negative streamwise velocity regions ('ejections') are indicated with dashed contours. The streamwise velocity fluctuations eventually decay, after the streamwise vorticity inducing them is sufficiently reduced.

For the uncontrolled cases, of course, $T_{uw} = 0$. For case (i), as the uncontrolled system is unstable, $||T_{xw}||_2$ and $||T_{xw}||_{\infty}$ are infinite; any slight excitation of the unstable mode of the system results in an unbounded response. For case (ii), the uncontrolled system has $||T_{xw}||_2 = 524.8$ and $||T_{xw}||_{\infty} = 15388$. Note that these numbers are quite large; due to the non-orthogonality of the eigenvectors of case (ii), the state is very sensitive to small disturbances of a particular structure. Note also that the system response

Control type	Control parameters	$ \boldsymbol{T}_{xw} _2$	$ m{\mathcal{T}}_{xw} _{\infty}$	$\max_{\tau,x(0)} \left\{ \frac{\mathscr{E}(\tau)}{\mathscr{E}(0)} \right\}$	$ \boldsymbol{T_{uw}} _2$
(No control)	_	∞	∞	∞	0
\mathcal{H}_2 Full control informatio $\gamma \to \infty$ controller		589.8 574.8 522.0 498.5 497.2 497.2	13357 12421 9163 7114 6673 6668	24.4 24.4 23.9 23.5 23.4 23.5	20.29 20.31 20.93 22.44 23.07 23.08
State estimator†	$\alpha = 1000$ $\alpha = 100$ $\alpha = 10$ $\alpha = 1$ $\alpha = 0.1$	461.6 339.0 133.8 89.2 90.1	10248 5273 563 160 158	55.5 53.4 33.4 25.4 25.4	0 0 0 0
Composite estimator/ controller:	$\alpha = 10, \ell = 30$	867.3 548.5 501.2	22565 9879 6730	57.2 47.8 50.4	24.05 20.94 23.17
\mathcal{H}_{∞} Full informatio $\alpha = 10$ controller $\ell = 30$	$ \gamma = \infty n $	522.0 538.8 884.1 1807.9 16522.7	9163 5129 4254 4091 4052	23.9 23.3 23.3 23.3 23.2	20.93 28.35 50.53 104.54 956.87
State estimator†	$\begin{array}{l} \gamma = \infty \\ \gamma = \gamma_0 = 704 \end{array}$	133.8 117.6	563 310	33.4 22.5	0 0
Composite estimator/controller:	$\gamma_{controller} = 8500$	548.5 1047.2	9879 4543	47.8 335.8	20.94 60.07
Proportional control $\phi_1 = \phi_2 = 0$	$k_1 = k_2 = 2\P$ $k_1 = k_2 = 10$ $k_1 = k_2 = 60$ $k_1 = k_2 = 100$ $k_1 = k_2 = 1000$ $k_1 = k_2 = 10000$	3549 4641 6993 7908 17596 43736	62248 6047 4577 5253 61341 456491	8.5 167 7410 17800 58600 86800	& & & & & & & &

[†] State estimator: transfer function to x_E and max growth of $\mathscr{E} \equiv x_E^* \ \mathbf{Q} \ x_E$ reported.

Table 3. Performance of various controllers, case (i): $Re = 10\,000$, $k_x = 1$, $k_z = 0$.

for the two different types of disturbances (Gaussian and worst case) differ by a factor of 30; Gaussian analysis alone is not sufficient to completely characterize the system.

6. Analysis of closed-loop systems

The controlled ('closed-loop') systems are now examined in detail using the analysis methods of §4. Specifically, the behaviour of the flow and the estimator/controllers (or portions thereof) operating together as a single dynamical system is characterized.

[‡] Composite estimator/controller: max growth of $\mathscr{E} \equiv x^* \mathbf{Q} x + x_E^* \mathbf{Q} x_E$ reported.

[¶] The minimum k_i which stabilize the proportionally controlled closed-loop system.

Con	trol type	Control parameters	$ \boldsymbol{\mathcal{T}}_{xw} _2$	$ m{T}_{xw} _{\infty}$	$\max_{\tau,x(0)} \left\{ \frac{\mathscr{E}(\tau)}{\mathscr{E}(0)} \right\}$	$ \boldsymbol{T_{uw}} _2$
(No	control)	-	524.8	15388	4897	0
$\begin{array}{c} \mathscr{H}_2 \\ \text{control} \\ \gamma \to \infty \end{array}$	Full information controller	$\ell = 1000$ $\ell = 100$ $\ell = 30$ $\ell = 10$ $\ell = 1$	523.2 426.5 284.8 22.61 212.6	15307 10796 5163 3616 3353	4858 943 155 185 161	0.03 1.93 6.35 11.59 18.25
	State estimator†	$\ell = 0.1$ $\alpha = 1000$ $\alpha = 100$ $\alpha = 30$ $\alpha = 10$ $\alpha = 1$ $\alpha = 0.1$	212.6 524.6 507.6 415.7 271.8 155.9 248.7	3350 15376 14333 9412 4853 2450 2383	159 4894 4667 3448 1779 762 690	18.49 0 0 0 0 0 0
	Composite estimator/controller‡	$ \alpha = 100, \ell = 100 \alpha = 10, \ell = 30 \alpha = 1, \ell = 1 $	522.4 398.8 271.3	15135 7988 4528	4844 2679 1313	0.07 3.49 15.50
\mathcal{H}_{∞} control $\alpha = 10$	Full information controller	$ \gamma = \infty \\ \gamma = \gamma_0 = 5340 $	284.8 260.8	5163 3558	155 277	6.35 8.86
$\ell = 30$	State estimator†	$ \gamma = \infty \gamma = \gamma_0 = 5058 $	271.8 234.5	4853 3284	1779 1473	0 0
	Composite estimator/controller‡	$ \begin{array}{l} \gamma = \infty \\ \gamma_{controller} = 5340 \\ \gamma_{estimator} = 5058 \end{array} \right\} $	398.8 353.2	7988 5797	2679 2357	3.49 5.56
Proportion control $\phi_1 = \phi_2$		$k_1 = k_2 = 0.1$ $k_1 = k_2 = 1$ $k_1 = k_2 = 10$ $k_1 = k_2 = 100$ $k_1 = k_2 = 1000$ $k_1 = 10, k_2 = 0$	543 1685 16175 161680 1616300 11443	15028 12885 9219 8181 8058 13405	4821 4327 3270 2095 2860 4219	& & & & & & &

[†] State estimator: transfer function to x_E and max growth of $\mathscr{E} \equiv x_E^* \mathbf{Q} x_E$ reported.

Table 4. Performance of various controllers, case (i): Re = 5000, $k_x = 0$, $k_z = 2.044$.

6.1. Quantitative comparison of various closed-loop systems

Tables 3 and 4 summarize a parametric study of a variety of control schemes applied to cases (i) and (ii), respectively, using the transfer function norms described in §4.4 to provide a quantitative comparison between \mathcal{H}_2 , \mathcal{H}_{∞} , and proportional controllers.

The first two columns in these tables list the settings of the relevant parameters used to determine the controller and/or estimator. The remaining columns contain data on the response of the state in the closed-loop system to Gaussian disturbances and worst-case disturbances, the maximum transient energy growth, and the level of control effort used to attain this closed-loop performance. Specifically, the third

[‡] Composite estimator/controller: max growth of $\mathscr{E} \equiv x^* \mathbf{Q} x + x_E^* \mathbf{Q} x_E$ reported.

column contains $||T_{xw}||_2$, which indicates the square-root of the expected energy of the state, $E[x^*Qx]$, in response to white Gaussian disturbances w. The fourth column contains $||T_{xw}||_{\infty}$, which indicates the square-root of the expected energy of the state in response to worst-case disturbances w with unit norm. For comparison, the fifth column contains the maximum transient energy growth of the closed-loop system. The sixth column contains $||T_{uw}||_2$, which indicates the r.m.s. value of the control u in response to white Gaussian disturbances w. Recall that, by (4.8), $||T_{zw}||_2^2 = ||T_{xw}||_2^2 + \ell^2 ||T_{uw}||_2^2$. For consistency, all transfer function norms tabulated are computed under the assumption that $\alpha = 1$ in the determination of the norm, though the estimator feedback L is determined with the value of α cited in the table. Of course, the analyses may be conducted easily for other values of α which better describe a particular system of interest.

6.1.1. Full information controllers

To investigate the behaviour of the \mathcal{H}_2 and \mathcal{H}_∞ controllers separately from that of the estimator, consider the closed-loop system 2 in (4.10) for the controlled state x, obtained by combining the open-loop plant with the controller and assuming full state information is available.

It is seen from tables 3 and 4 that full information controllers do an excellent job of reducing both $||T_{xw}||_2$ and $||T_{xw}||_\infty$, while maintaining finite values of $||T_{uw}||_2$. The full information \mathcal{H}_2 controllers minimize the 2-norm of the transfer function from the disturbance w to the performance measure z, namely, $||T_{zw}||_2^2 = ||T_{xw}||_2^2 + \ell^2||T_{uw}||_2^2$; this is, in fact, the \mathcal{H}_2 design objective. As the control is made cheaper (ℓ is reduced), the state x contributes relatively more to the performance measure z, causing the \mathcal{H}_2 controller to drive $||T_{xw}||_2$ to the minimum value possible, though the control effort required, $||T_{uw}||_2$, generally increases; these trends are all confirmed in the tables.

At a fixed price for the control ($\ell=30$), the introduction of a worst-case disturbance in the design of an \mathscr{H}_{∞} controller (by the reduction of γ) results in a system which does not necessarily further reduce $||\mathbf{T}_{xw}||_2$, but which reduces the ∞ -norm of the transfer function from the disturbance w to the performance measure z, namely, $||\mathbf{T}_{zw}||_{\infty}$; this is, in fact, the \mathscr{H}_{∞} design objective. For vanishing values of ℓ , the absolute minimum value for $||\mathbf{T}_{xw}||_{\infty}$ may be obtained by reducing γ of the \mathscr{H}_{∞} controller to its minimum value γ_0 . However, such a controller may require more control effort, $||\mathbf{T}_{uw}||_2$, and/or have worse response to Gaussian disturbances, $||\mathbf{T}_{xw}||_2$, than desirable for a particular implementation. To compensate, intermediate values of γ and ℓ may be chosen. The two parameters γ and ℓ provide the flexibility needed to achieve the desired trade-off between (a) Gaussian disturbance response, (b) worst-case disturbance response, and (c) control effort required.

Note that $\ell \to 0$ limits exist for all norms listed for both case (i) and case (ii). As the present systems are stabilizable but not controllable, as remarked in § 5.1, there are diminishing returns to be gained by increasing the feedback gains K. The optimal controllers do not attempt to push the closed-loop system beyond the limits imposed by uncontrollable modes. This topic is quantified further in § 6.5 using the modal control residuals defined in § 4.2.

6.1.2. State estimators

To investigate the behaviour of the \mathcal{H}_2 and \mathcal{H}_{∞} estimators separately from that of the controller, consider the closed-loop system 3 in (4.11) for the estimation error $x_E \equiv x - \hat{x}$, obtained by combining the open-loop plant with the estimator and assuming no control is applied.

It is seen from tables 3 and 4 that the state estimators (based on measurements at the wall only) do an excellent job of regulating the response of the estimation error x_E to both Gaussian disturbances ($||T_{xw}||_2$) and worst-case disturbances ($||T_{xw}||_{\infty}$). As the measurements are assumed to be increasingly accurate in the design of the estimator (α is reduced), the estimator feedback is increased, and it is seen that the \mathcal{H}_2 estimator drives $||T_{xw}||_2$ to small values, though the estimator feedback (not tabulated) generally increases. Note that the behaviour of $||T_{xw}||_2$ is not quite monotonic with respect to α for both case (i) and case (ii). This is because the \mathcal{H}_2 estimator is designed to reduce the expected value of $x_E^* x_E$, though, in the tables, $||T_{xw}||_2$ represents the transfer function related to the expected value of $x_E^* \mathbf{Q} x_E$ for consistency. The difference between these two types of measures is discussed further in § 6.2.

At a fixed relative magnitude of measurement noise, $\alpha=10$, the introduction of a worst-case disturbance in the design of an \mathscr{H}_{∞} estimator (by the reduction of γ) results in a system which reduces $||\mathbf{T}_{zw}||_{\infty}$, in a manner analogous to that of the \mathscr{H}_{∞} controller. For small values of α (reliable measurements), high levels of estimator feedback may result. Note that high levels of estimator feedback (or, for that matter, controller feedback) can cause problems if the state model \mathbf{A} in the estimator (3.2a) is inaccurate. Though this topic is beyond the scope of the present discussion, it suffices to say that small levels of estimator feedback are desirable from the standpoint of reduced sensitivity to modelling errors. The two parameters γ and α provide the flexibility needed to achieve the desired trade-off between (a) Gaussian disturbance response, (b) worst-case disturbance response, and (c) estimator feedback required. Future work recommended in this area would be a μ -synthesis approach to the present control problem to account rigorously for the sensitivity of the system to modelling uncertainties (Skogestad & Postlethwaite 1996).

6.1.3. Composite estimator/controllers

To investigate the behaviour of the estimator and controller acting together, consider the closed-loop composite system 4 in (4.12), in which the state is formed by the union of x and x_E and the system is obtained by combining the open-loop plant with both the estimator and the controller. It is seen from tables 3 and 4 that the transfer function norms $||T_{xw}||_2$ and $||T_{xw}||_\infty$ for the controlled systems based on estimated state information \hat{x} are slightly degraded from the controlled systems using the corresponding full-information controllers.

Some degradation of performance in the composite system (as compared with the full-information system) is expected, as the system dynamics of the composite system are of increased complexity. To characterize the dynamics of the composite system when no disturbances are present, the eigenmodes of

$$\tilde{\mathbf{A}} = \begin{pmatrix} \mathbf{A} + \mathbf{B}_2 \, \mathbf{K} & -\mathbf{B}_2 \, \mathbf{K} \\ 0 & \mathbf{A} + \mathbf{L} \, \mathbf{C}_2 \end{pmatrix}$$

may be considered. The closed-loop eigenvalues of the composite system matrix $\tilde{\mathbf{A}}$ are simply the union of the eigenvalues of the controlled system $(\mathbf{A} + \mathbf{B}_2 \mathbf{K})$ and the eigenvalues of the estimated system $(\mathbf{A} + \mathbf{L} \mathbf{C}_2)$ discussed in the previous two Sections.

Half of the eigenvectors of $\tilde{\mathbf{A}}$ are formed by the eigenvectors of the controlled system $(\mathbf{A} + \mathbf{B}_2 \mathbf{K}) x = \lambda x$ with $x_E = \mathbf{0}$. Thus, in the closed-loop composite system with no disturbances, if the initial state estimate is correct $(x_E(0) = \mathbf{0})$, then the state estimate will remain correct $(x_E(t) = \mathbf{0})$ and the dynamics of the (decoupled)

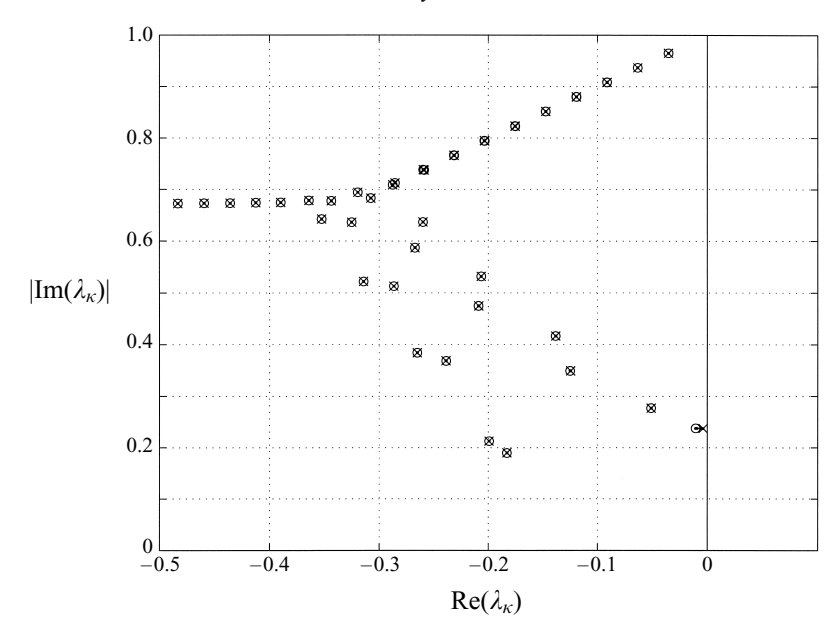


FIGURE 5. Locus of least-stable eigenvalues of the \mathscr{H}_2 controller $(\gamma \to \infty)$ as a function of ℓ . Eigenvalues for $\ell \to \infty$ are marked with an \times , and those for $\ell \to 0$ are marked with an o. Note that eigenvalues barely move in this plot, though $||T_{zw}||_2$, for which this controller is designed, is effectively minimized.

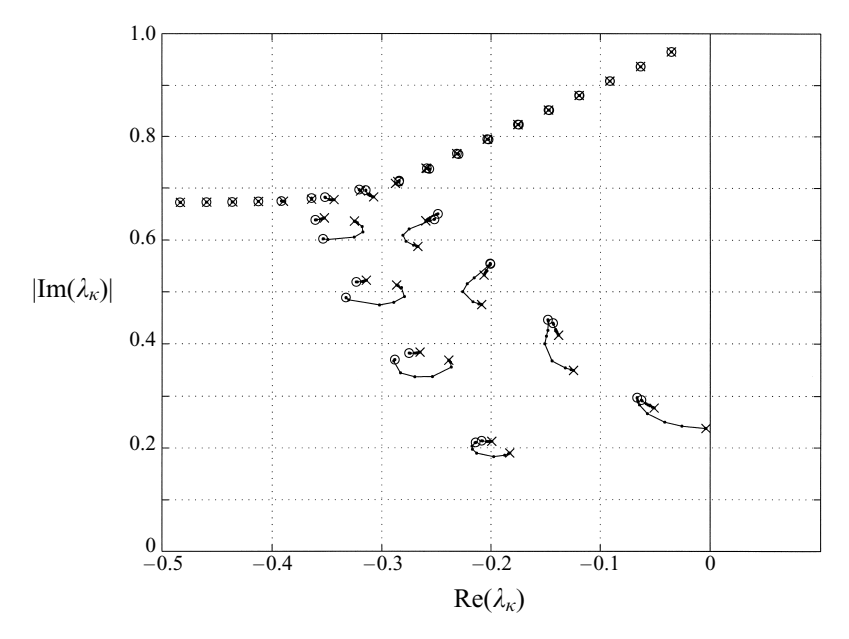


FIGURE 6. Locus of least-stable eigenvalues of a modified \mathcal{H}_2 controller, taking (for this plot only) $\mathbf{C}_1 = (\mathbf{I} \quad \mathbf{0})^*$. Eigenvalues are marked as in figure 5. Note that the eigenvalues in the lower branch are significantly moved by this modified \mathcal{H}_2 controller. However, the physically relevant transfer function norms are more effectively reduced by controllers which are specifically designed taking the energy of the state into account, i.e. by those which take $\mathbf{C}_1 = (\mathbf{Q}^{1/2} \ \mathbf{0})^*$. As shown in figure 5, such controllers may result in significantly less eigenvalue movement in a root locus plot. This implies that root locus plots themselves, which characterize eigenvalues but not eigenvectors or closed-loop transfer function norms, do not give the complete picture of system performance.

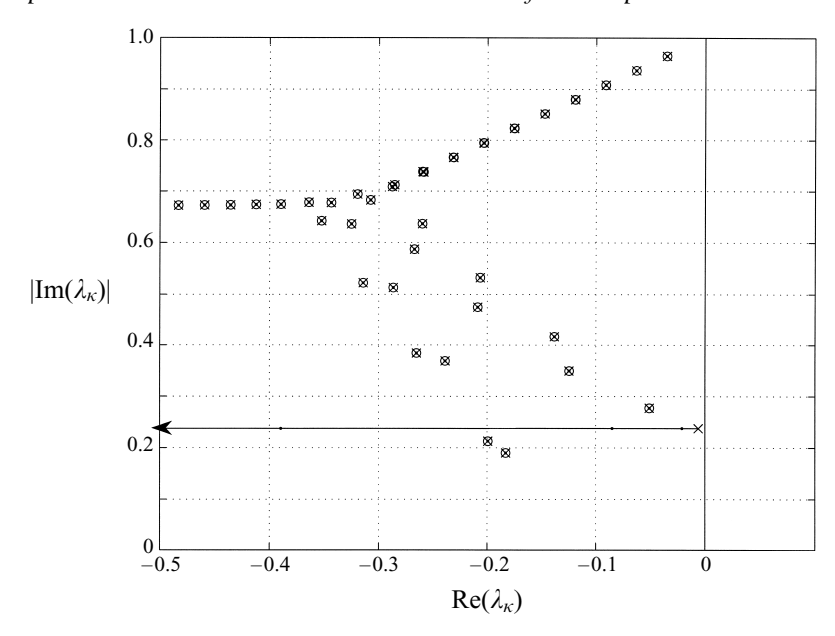


FIGURE 7. Locus of least-stable eigenvalues of the \mathscr{H}_{∞} controller as a function of γ , taking $\ell=30$. Eigenvalues for the \mathscr{H}_2 limit $(\gamma\to\infty)$ are marked with an \times , and those for $\gamma\to\gamma_0$ are marked with an o. The introduction of the unstructured disturbance in the \mathscr{H}_{∞} controller modifies only the least-stable eigenmode of an \mathscr{H}_2 result, without expending any extra feedback to control those eigenmodes not associated with the maximally unstable component of the system.

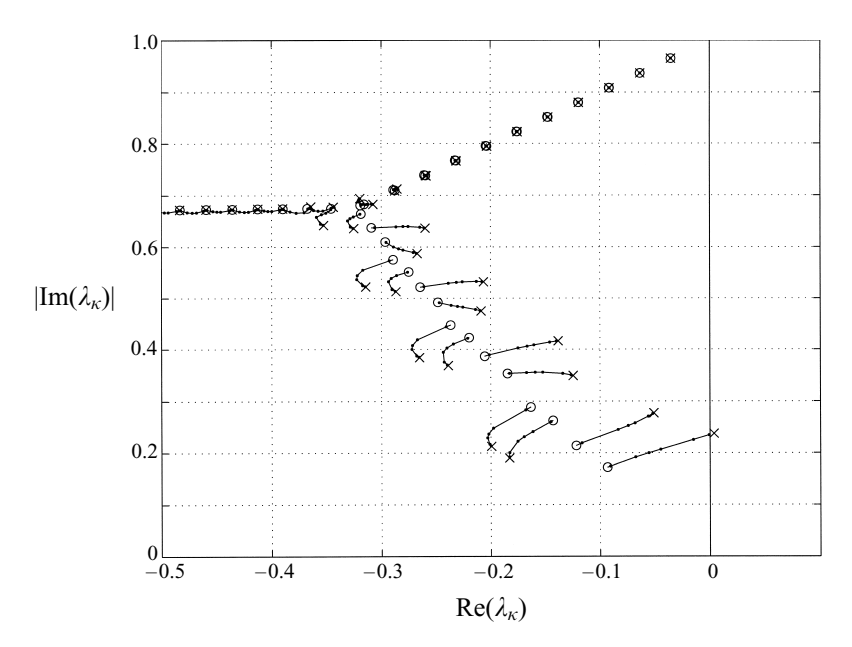


FIGURE 8. Locus of least-stable eigenvalues of the MIMO proportional controller as a function of $k_1 = k_2 = k$, taking $\phi_1 = \phi_2 = 0$. Eigenvalues for k = 0 are marked with an \times , and those for $k \to \infty$ are marked with an o. Note that, in the large gain limit, the eigenvalues in the lower branch align on a diagonal line.

system as it is regulated to zero will simply be the dynamics of the controlled plant provided with full state information. The other half of the eigenvectors of $\tilde{\bf A}$ are formed by the eigenvectors of the estimated system $({\bf A}+{\bf L}\,{\bf C}_2)\,x_E=\lambda\,x_E$ with ${\bf x}=({\bf A}+{\bf B}_2\,{\bf K}-\lambda{\bf I})^{-1}\,{\bf B}_2\,{\bf K}\,x_E$. Thus, any errors in the initial state estimate $(x_E(0)\neq {\bf 0})$ will induce perturbations in the state itself $(x(t)\neq {\bf 0})$ as the entire coupled system is regulated back to zero.

6.1.4. Comparison with proportional control

Proportional controllers, though simpler in their design, are not nearly as effective as the \mathcal{H}_2 and \mathcal{H}_{∞} controllers. The most important flaw of any controller with a proportional component, as described in §4.6, is that it has no high-frequency roll-off in the controller's response to measurement noise, so the r.m.s. of the control response u to white noise ($||T_{uw}||_2$) is unbounded.

The best \mathcal{H}_{∞} composite estimator/controllers tested, shown in tables 3 and 4, are seen to perform better than all proportional controllers tested with respect to the response of the state x to both white noise disturbances ($||\mathbf{T}_{xw}||_2$) and worst case disturbances ($||\mathbf{T}_{xw}||_{\infty}$). This is remarkable, as the \mathcal{H}_{∞} estimator/controllers use significantly less control energy than the proportional controllers, as indicated by their bounded values of $||\mathbf{T}_{uw}||_2$.

6.2. System eigenvalue ('root locus') analyses

By examining root locus plots which map the movement of the closed-loop system eigenvalues with respect to the scalar parameters of the system (for the \mathscr{H}_{∞} controller, γ , α , or ℓ ; for the proportional controller, $k_1 = k_2 = k$), the effect of an estimator/controller applied to a large MIMO linear system may be partially characterized.

The eigenmodes of $\tilde{\mathbf{A}} = \mathbf{A} + \mathbf{B}_2 \mathbf{K}$ describe the dynamics of the closed-loop system 2 in (4.10) when $\mathbf{u}' = \mathbf{w} = \mathbf{0}$. The movement of these eigenvalues as a function of ℓ and γ , the free parameters of the \mathcal{H}_{∞} controller, for case (i) are examined in figures 5, 6 and 7. The eigenvalues for $\ell \to \infty$ are very near those of the uncontrolled system \mathbf{A} in figures 5 and 6, with the previously unstable mode reflected just to the left of the imaginary axis; this solution represents the 'expensive control' limit that uses the minimum control necessary to marginally stabilize the system. The eigenvalues generally move to the left as ℓ , the 'price' of the control, is decreased.

For $\mathbf{C}_1 = (\mathbf{Q}^{1/2} \mathbf{0})^*$, the definition given in (3.4) and used throughout this paper, the root locus for an \mathcal{H}_2 controller with respect to ℓ is given in figure 5; note that the eigenvalues move only slightly with the application of \mathcal{H}_2 control. For $\mathbf{C}_1 = (\mathbf{I} \ \mathbf{0})^*$, a definition which weights all of the discretized values of the state x equally, more eigenvalue movement is seen in the root locus with respect to ℓ , as shown in figure 6. However, the physically relevant energy norm, $||T_{zw}||_2$, is reduced less effectively by this modified \mathcal{H}_2 controller. The modified definition of \mathbf{C}_1 results in extra weighting in the performance measure on those regions of flow where the grid points are clustered. In the present case, this weighting takes the form $\eta(y) = (1 - y^2)^{-1/2}$, as discussed in § 2.4. This is a very large weighting on the eigenfunctions near the wall, and thus this performance measure results in very large movement of all of the controllable eigenmodes which are non-zero in the heavily weighted region near the wall when the corresponding optimal controller is applied. The weighting given by $\eta(y)$ is not physically based, and thus, in the opinion of the authors, should not be used to define the performance measure. If a rigorous analysis indicates a Lyapunov function more relevant to secondary instability than the energy norm, that function may easily be used to replace Q in the present development. However, the *ad hoc* weighting implied by $\eta(y)$ is almost certainly not such a function, and performance measures based on the kinetic energy density, as used here, are preferred.

Figure 7 shows the movement of the closed-loop system eigenvalues as a function of γ , taking $\ell=30$. Starting from a stable closed-loop \mathscr{H}_2 system ($\gamma=\infty$) with an intermediate value for the price of the control ($\ell=30$), it is observed that the introduction of an unstructured disturbance into the controller computation (reducing γ) affects only the least-stable component of the system. Compare this with the \mathscr{H}_2 controller in figures 5 and 6, which show that all controllable modes of the system are modified when ℓ is reduced.

Figure 8 shows the movement of the closed-loop system eigenvalues when MIMO proportional control is applied. For $k \ge 2$, the system is stable (i.e. the unstable eigenvalue moves to the left half-plane), and the eigenmodes appear to be effectively controlled right up to the large gain limit. Note also that a new, distinct (\prec)-shaped structure to the locus of eigenvalues emerges for case (i) with a MIMO proportional controller in the large gain limit, as indicated by the eigenvalues marked with an o in figure 8. The simple pattern of eigenvalues in the lower branch, which is reminiscent of the pattern of eigenvalues of the (uncontrollable) centre modes in the upper branch, apparently emerges due to a fundamental shift to a simple boundary condition in this limit, as discussed in the following section.

Though root locus plots do reveal some important trends, they do not indicate the important effects of the non-orthogonality of the eigenvectors or the effect of the control on the physically relevant norms of interest. For systems (such as the present) with highly non-orthogonal eigenvectors, a root locus characterization can therefore be misleading, as established above by the apparently good behaviour of the proportional controller in the large gain limit, indicated by figure 8, but its terrible disturbance response in this limit, reported in table 3. Note that Trefethen *et al.* (1993) have proposed an interesting extension to the root locus approach, referred to as pseudospectra, which extends the root locus analysis to reflect the sensitivity of a system to external forcing. In the future, such a technique should be explored in a closed-loop framework in an attempt to obtain a graphical characterization of different control approaches.

6.3. Modification of eigenvectors by application of control

The modified shapes of the closed-loop eigenvectors for case (i) by application of \mathscr{H}_{∞} control and proportional control are shown in figure 9. Only the $\kappa=1$ mode is significantly modified by the \mathscr{H}_{∞} controller, whereas all controllable eigenmodes are modified by the proportional controller. For case (ii), however, it is seen that the \mathscr{H}_2 (and \mathscr{H}_{∞}) controllers modify all of the eigenvectors, as shown in figure 10. In this case, the critical issue is the non-orthogonality of the set of eigenvectors, not the real component of any particular eigenvalue, and thus the optimal control acts to make the set of eigenvectors more orthogonal.

Recall from § 2 that the boundary conditions on the uncontrolled Orr-Sommerfeld problem are v=0 and $\partial v/\partial y=0$ at the walls. Consider the proportional controller of the form $\mathbf{u}=\mathbf{K}\mathbf{y}_m$ given in (3.7), taking $k_1=k_2=k$ and $\phi_1=\phi_2=\phi$. By (2.5), noting that $k_z=0$ for this case, the homogeneous Dirichlet boundary conditions at each wall are replaced by

$$v = k e^{i\phi} \frac{1}{Re} \frac{\partial u}{\partial y} = k \left(\frac{i k_x e^{i\phi}}{k_x^2 + k_z^2} \frac{1}{Re} \right) \frac{\partial^2 v}{\partial y^2} = k C \frac{\partial^2 v}{\partial y^2},$$

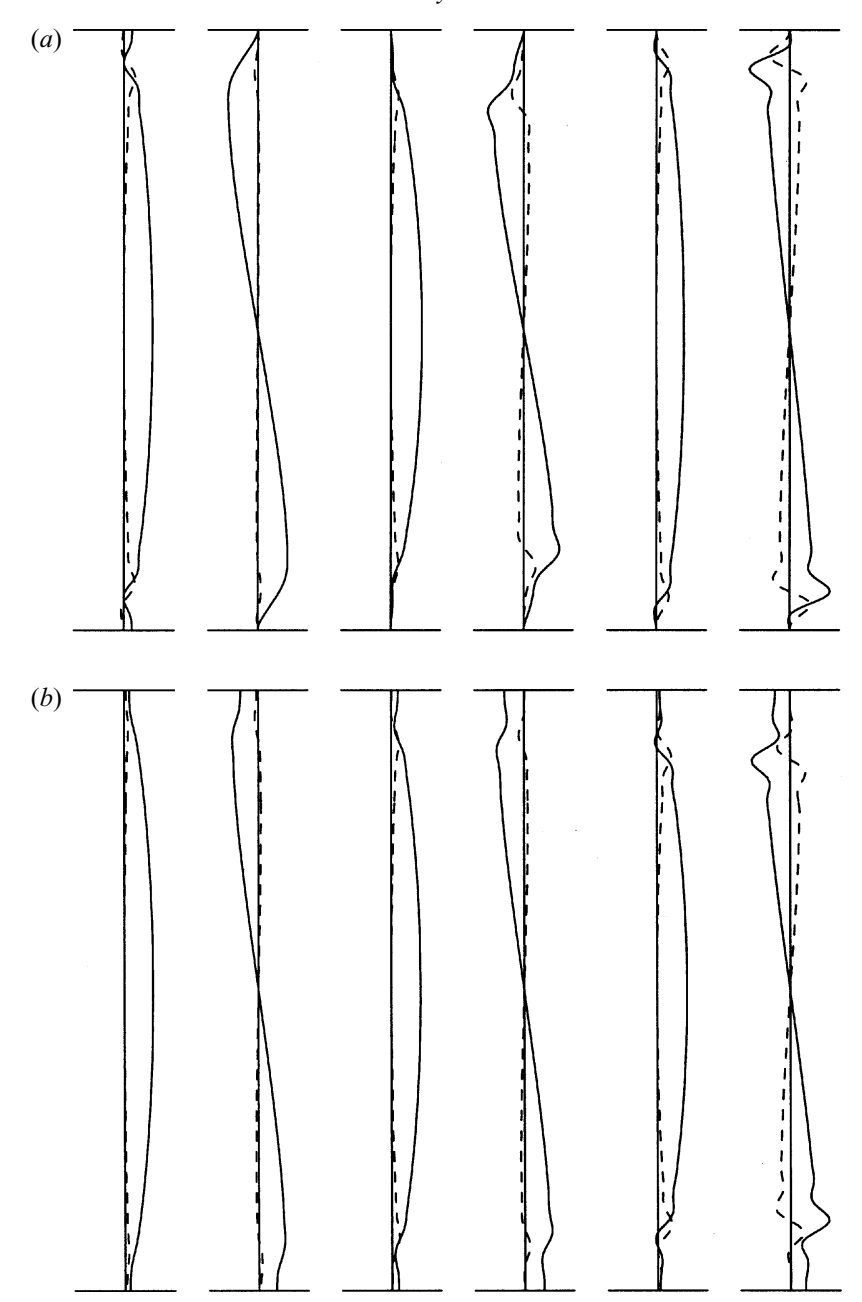


FIGURE 9. Modified shape of closed-loop eigenvectors for case (i) by application of \mathcal{H}_{∞} control (a) and MIMO proportional control (b). Eigenvectors scaled as in figure 1(b). Note that only eigenvectors with wall support, corresponding to the six least-stable eigenmodes from the lower branch, are plotted; the uncontrollable eigenmodes from the upper branch are not modified by the control and are not shown. Those eigenmodes which have been modified by the control show a non-zero value of v at the wall in the above plots. (a) $\ell=30$ and $\gamma=8300$. Only the least-stable mode is significantly modified. (b) $k_1=k_2=10000$. All controllable eigenmodes are significantly modified.

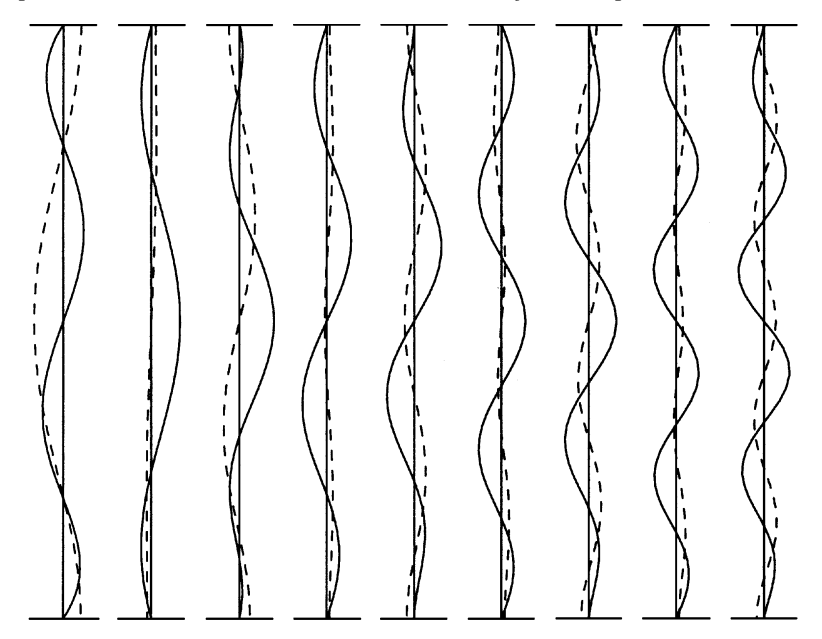


FIGURE 10. Modified shape of the nine least-stable closed-loop eigenvectors for case (ii) by application of \mathcal{H}_2 control with $\ell=1$. Eigenvectors plotted as in figure 2(b), with the v component (dashed) magnified by a factor of 300 rather than a factor of 1000. The eigenvectors are made more orthogonal by the application of control, to the point that a one-to-one correspondence of the above eigenmodes to the uncontrolled eigenmodes of figure 2(b) is barely distinguishable.

where C is some constant. Note that the homogeneous Neumann boundary condition still applies due to continuity. In the limit for which the feedback gain $k \to \infty$, assuming the eigenvectors remain finite (confirmed *a posteriori*), the Dirichlet boundary condition is equivalent to a homogeneous boundary condition on the second derivative of v, i.e.

$$\frac{\partial v}{\partial y} = 0$$
 and $\frac{\partial^2 v}{\partial y^2} = 0$ when $k \to \infty$.

These simple boundary conditions on the closed-loop eigenvectors are verified by the plots of the computed eigenvectors for the proportional controller with large k in figure 9(b) for case (i), which clearly shows that both the slope and the curvature of the closed-loop eigenvectors go to zero near the wall. It is inferred that these simple homogeneous boundary conditions are related to the simple eigenvalue structure which emerges in this limit, as shown in figure 8.

6.4. Reduction of maximum transient energy growth

The effect of the control on the worst-case transient energy growth is tabulated along with the transfer function norms in tables 3 and 4. Though large values of $||T_{zw}||_{\infty}$ and large values of transient energy growth are both due, in part, to non-orthogonality of the eigenvectors, they do not always correlate closely as the various control parameters are altered. It is the excitation by external disturbance forcing, and not the growth from a particularly deleterious set of initial conditions, which is the primary topic of interest in the present control problem. Thus, transfer function norms, which quantify the response of the state and the control to external disturbance forcing, are used in the

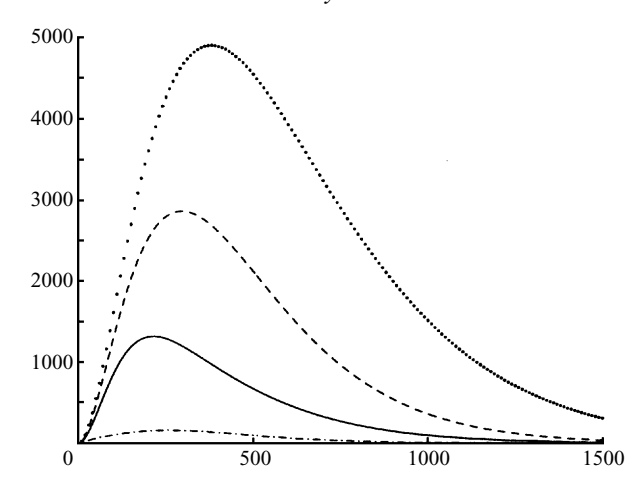


FIGURE 11. Reduction of maximum transient energy growth by application of control to case (ii): $\mathscr{E}(t)/\mathscr{E}(0)$ versus t. Top to bottom: no control, proportional control (k=1000), wall-information \mathscr{H}_2 control ($\gamma=\infty, \alpha=1, \ell=1$), full-information \mathscr{H}_2 control ($\gamma=\infty, \ell=30$).

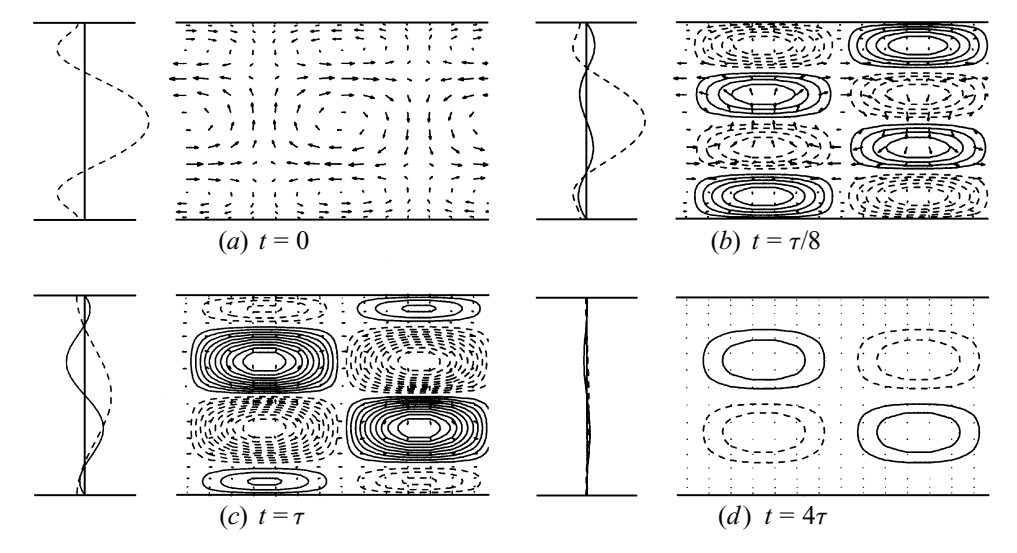


FIGURE 12. Shape of the modified flow perturbation with the largest transient energy growth for the closed-loop case (ii) with full-information \mathcal{H}_2 control. A thirty-fold reduction of transient energy growth is obtained (figure 11) as compared with perturbations to the uncontrolled flow (figure 4). Subfigures plotted as in figure 4, with the contours of streamwise velocity rescaled to show detail. The control at the wall acts to create small 'buffer' vortices near each wall, thereby reducing the extent of the streamwise vortex at the centre of the channel. The reduction in energy growth is compounded by the fact that this reduced centre vortex acts over a reduced range in mean streamwise velocity $U(y) = 1 - y^2$ between the centre and the edge of the vortex, thereby reducing its effectiveness at inducing streamwise velocity fluctuations.

present work to formulate the control objective. However, a side effect of the control application in the present problem is that the maximum transient energy growth of the system is reduced effectively. For example, the maximum transient energy growth in case (ii), which is reduced from an uncontrolled value of $\mathcal{E}(\tau)/\mathcal{E}(0) = 4897$ to a value of 2860 by the proportional controller, is reduced to a value of 1313 by the wall-information \mathcal{H}_2 controller, and is reduced to a value of 155 by the

κ	λ_{κ}	f_{κ}
1	-0.01047924 - 0.23786793i	0.000148105
2	-0.03516736 - 0.96463100i	0.000000125
3	-0.03518658 - 0.96464251i	0.000000003
4	-0.05096577 - 0.27721190i	0.000015360
5	-0.06320167 - 0.93631678i	0.000000297
6	-0.06325157 - 0.93635179i	0.000000012
7	-0.09122298 - 0.90798352i	0.000000538
8	-0.09131286 - 0.90805636i	0.000000033
9	-0.11923315 - 0.87962804i	0.000000918
10	-0.11937073 - 0.87975574i	0.000000072
11	-0.12496333 - 0.34921218i	0.000106622
12	-0.13828462 - 0.41636473i	0.000021774
13	-0.14723423 - 0.85124693i	0.000001639
14	-0.14742558 - 0.85144947i	0.000000156
15	-0.17522893 - 0.82283652i	0.000003228

TABLE 5. Least-stable eigenmodes of the closed-loop system $(\mathbf{A} + \mathbf{B}_2 \mathbf{K})$ and their sensitivity to modifications of the control rule for the \mathcal{H}_2 controller in the limit of cheap control $(\ell = 0.01)$. The numbering of the eigenvalues shown is the same as the numbering of the eigenvalues of table 1 to which they are connected by the root locus of figure 5. In the $\ell \to 0$ limit, the control feedback modifies the closed-loop system eigenmodes until they are insensitive to further modifications of the control feedback, as illustrated by vanishing values of the control residual f_{κ} .

full-information \mathcal{H}_2 controller, as tabulated in table 4 and shown in figure 11. The mechanism for the large reduction in energy growth is explained in physical terms in figure 12. Finite-horizon terminal controllers, in both an \mathcal{H}_2 and \mathcal{H}_∞ setting (Green & Limebeer 1995), may be proposed to minimize the transient energy growth of a closed-loop system over a time interval τ in a rigorous manner. However, such is not the objective of the present control problem.

6.5. Sensitivity of optimal estimator/controllers to further modification

The sensitivity of the closed-loop system eigenmodes to further modification of the \mathcal{H}_2 controller $(\gamma \to \infty)$ in the cheap control limit $(\ell \to 0)$ is shown in table 5. This table shows that, in the cheap control limit, the closed-loop system matrix is modified to the point that the eigenmodes are no longer sensitive to further modification of the controller feedback. All of the controllable dynamics of the system have been used by the controller feedback in this limit. This demonstrates that the optimal (\mathcal{H}_2) controller extracts the best possible performance from a given system assumed to have no state disturbances and full, accurate state information.

The sensitivity of the closed-loop system eigenmodes to further modification of the \mathscr{H}_2 estimator $(\gamma \to \infty)$ in the low measurement noise limit $(\alpha \to 0)$ is shown in table 6. This table shows that, in the limit of precise flow measurements, the closed-loop system matrix is modified to the point that the eigenmodes are no longer sensitive to further modification of the estimator feedback. All of the observable dynamics of the system have been used by the estimator feedback in this limit. This demonstrates that the optimal (\mathscr{H}_2) estimator (also known as a Kalman–Bucy filter) extracts the best possible state estimate from a given set of measurements when no control is applied and the system matrix \mathbf{A} is modelled exactly.

Note, however, that the locations of the closed-loop eigenvalues in the $\ell \to 0$ and $\alpha \to 0$ limits depend upon the definition of performance measure, and thus are

κ	λ_{κ}	$oldsymbol{g}_{\kappa}$
2	-0.03505745 - 0.96474092i	0.0000568
3	-0.03518656 - 0.96464253i	0.0000004
5	-0.06287933 - 0.93668082i	0.0000644
6	-0.06325135 - 0.93635193i	0.0000008
4	-0.08362192 - 0.25066956i	0.0002858
7	-0.09059623 - 0.90874809i	0.0000673
8	-0.09131193 - 0.90805687i	0.0000011
1	-0.09588644 - 0.17888614i	0.0000118
9	-0.11823783 - 0.88095109i	0.0000646
10	-0.11936798 - 0.87975705i	0.0000014
11	-0.14135187 - 0.25722461i	0.0000176
13	-0.14584721 - 0.85329546i	0.0000549
14	-0.14741907 - 0.85145213i	0.0000014
15	-0.17347709 - 0.82577391i	0.0000399
12	-0.17418704 - 0.40314739i	0.0002002

Table 6. Least-stable eigenmodes of the closed-loop system ($\mathbf{A} + \mathbf{LC}_2$) and their sensitivity to modifications of the estimator feedback for the \mathcal{H}_2 estimator in the limit of vanishing measurement noise ($\alpha = 0.000001$). The numbering of the eigenvalues shown is the same as the numbering of the eigenvalues of table 1 to which they are connected by the appropriate root locus with respect to α . In the $\alpha \to 0$ limit, the estimator feedback modifies the closed-loop system eigenmodes until they are insensitive to further modifications of the estimator feedback, as illustrated by vanishing values of the observation residual \mathbf{g}_{κ} .

not unique. This can be seen by noting that, in the $\ell \to 0$ limit, the eigenvalue locations obtained by the two optimal controllers in figures 5 and 6 are very different. Thus, though the modal control and observation residuals f_{κ} and g_{κ} are useful from a qualitative standpoint to understand the limiting processes involved, they do not provide quantitative measures for how far a given eigenvalue will move upon application of control.

7. Summary and conclusions

Optimal (\mathcal{H}_2) and robust (\mathcal{H}_∞) control theories have been applied to the equations governing linear instabilities and disturbance amplification in laminar flows. Two cases, one supercritical and one subcritical (with highly non-orthogonal eigenmodes), have been studied in detail. The disturbance response in both cases is effectively reduced by the modern control approaches, and it is shown that approaches based on modern control theory significantly outperform classical proportional control approaches. Several different analysis approaches are used to quantify the behaviour of the controlled systems. Transfer function norms are the most natural measure to characterize the relevant properties of the systems at hand. Maximum transient energy growth also characterizes eigenmode non-orthogonality, but does not characterize well the degree to which external disturbances excite flow perturbations. Root locus analyses alone, which account only for system eigenvalues and not the non-orthogonality of system eigenvectors, are inadequate to characterize the present systems.

A convenient new scaling to the \mathcal{H}_{∞} estimation problem has been introduced such that three scalar parameters $\{\gamma, \alpha, \ell\}$ may be individually adjusted to achieve desired closed-loop system characteristics in large MIMO systems, and the performance of a

family of \mathcal{H}_2 and \mathcal{H}_∞ controllers applied to the flow stability problem is thoroughly characterized. With this new scaling, the magnitude of α required for good estimator performance is a quantitative measure of how 'clean' the measurements have to be (relative to the magnitude of the state disturbances) to achieve the desired closed-loop performance of the \mathcal{H}_2 estimator. The dual structure of the control and estimation problems is retained with this scaling, clearly indicating the coupling and decoupling of the two problems as the three scalar parameters are varied.

Given control of the wall-normal component of boundary velocity only, the flow system is found to be stabilizable but not controllable. Given measurements of wall skin-friction only, the flow system is found to be detectable but not observable. It is shown that \mathcal{H}_2 estimators and controllers maximize closed-loop system performance with respect to Gaussian disturbances by minimizing the 2-norm of the transfer function from the disturbances w to an appropriate performance measure z, denoted $||T_{zw}||_2$. In contrast, \mathcal{H}_{∞} estimators and controllers modify the corresponding \mathcal{H}_2 systems in their response to worst-case disturbances by bounding the ∞ -norm of the transfer function from the disturbances to the performance measure, denoted $||T_{zw}||_{\infty}$. Reducing γ to the minimum value γ_0 for which a solution to the resulting Riccati equations exists results in the minimization of $||T_{zw}||_{\infty}$.

By reducing γ , the structured disturbance term of an \mathscr{H}_{∞} estimator/controller identifies and stabilizes the response of the corresponding \mathscr{H}_2 closed-loop system to the particular disturbance to which it is most sensitive, and thus uses smaller amounts of feedback to attain the same level of worst-case system performance than would be necessary by reducing ℓ or α alone. Such reduced feedback results in smaller demands on the actuators used to achieve the closed-loop forcing and improved robustness to inaccuracies in the system model; the reduced feedback applied in the \mathscr{H}_{∞} approach results in reduced opportunity for improper feedback to disrupt the closed-loop system. Together, the scalar parameters $\{\gamma,\alpha,\ell\}$ provide a large degree of flexibility in the design of the \mathscr{H}_{∞} estimator/controllers to obtain the best trade-offs possible in the closed-loop systems between Gaussian disturbance response, worst-case disturbance response, and feedback levels required.

This work was begun at the 1996 Summer Program of the Center for Turbulence Research at Stanford University in close collaboration with Professor Ramesh Agarwal. The authors also thank Professors Parviz Moin and Steven Crow for direction during the genesis of this project, Professor Alan Laub for advice on the numerical approach to the Riccati equation, Professor S. Scott Collis for recommending the weak formulation for the Neumann b.c., Dr Jeffrey Baggett for recommending the treatment of the spurious eigenvalues, Dr R. K. Owen for assistance with the numerical implementation in quad precision, and Dr Krishnan Mahesh, Dr Mohammed Ziane, and Capt. Danforth Bewley for fruitful discussions and detailed comments on a draft copy of this manuscript. The financial support of the Air Force Office of Scientific Research, the Center for Turbulence Research, and GM Powertrain (Transmission Group), and the computer time provided by NASA Ames Research Center, are gratefully acknowledged.

REFERENCES

- ABERGEL, F. & TEMAM, R. 1990 On some control problems in fluid mechanics. *Theor. Comput. Fluid Dyn.* 1, 303–325.
- ANDERSON, E., BAI, Z., BISCHOF, C., DEMMEL, J., DONGARRA, J., DU CROZ, J., GREENBAUM, A., HAMMARLING, S., MCKENNEY, A., OSTROUCHOV, S. & SORENSEN, D. 1995 *LAPACK Users' Guide*, SIAM.
- BAMIEH, B. 1997 The structure of optimal controllers of spatially-invariant distributed parameter systems. *Proc. 36th IEEE Conf. on Decision and Control, Dec 8–12, San Diego.*
- Bartels, R. H. & Stewart, G. W. 1972 Solution of the matrix equation AX + XB = C. Commun. ACM 15, 820–826.
- Bewley, T. R. & Agarwal, R. 1996 Optimal and robust control of transition. *Proc. 1996 CTR Summer Program*. Center for Turbulence Research, Stanford University/NASA Ames.
- Bewley, T. R., Moin, P. & Temam, R. 1997 Optimal and robust approaches for linear and nonlinear regulation problems in fluid mechanics. *AIAA Paper* 97-1872.
- Bewley, T. R., Temam, R. & Ziane, M. 1998 A generalized framework for robust control in fluid mechanics. Accepted for publication in *Physica D*.
- Bridges, T. J. & Morris, P. J. 1984 Differential eigenvalue problems in which the parameter appears nonlinearly. *J. Comput. Phys.* 55, 437–460.
- Butler, K. M. & Farrell, B. F. 1992 Three-dimensional optimal perturbations in viscous shear flows. *Phys. Fluids* A **4**, 1637–1650.
- CANUTO, C., HUSSAINI, M. Y., QUARTERONI, A. & ZANG, T. A. 1988 Spectral Methods in Fluid Dynamics. Springer.
- Dailey, R. L., Doyle, J. C., Stein, G., Banda, S. S. & Yeh, H. H. 1990 Lecture Notes for the Workshop on \mathcal{H}_{∞} and μ Methods for Robust Control. Presented at 1990 American Control Conference, May 21–22, San Diego.
- Doyle, J. C., Francis, B. A. & Tannenbaum, A. R. 1992 Feedback Control Theory. Macmillan.
- Doyle, J. C., Glover, K., Khargonekar, P. P. & Francis, B. A. 1989 State-space solutions to standard \mathcal{H}_2 and \mathcal{H}_{∞} control problems. *IEEE Trans. Auto. Control* **34**, 831–847.
- Drazin, P. G. & Reid, W. H. 1981 Hydrodynamic Stability. Cambridge University Press.
- Franklin, G. F., Powell, J. D. & Emami-Naeini, A. 1991 Feedback Control of Dynamic Systems. Addison-Wesley.
- Grace, A., Laub, A. J., Little, J. N. & Thompson, C. M. 1992 Control System Toolbox User's Guide. The MathWorks, Inc.
- GREEN, M. & LIMEBEER, D. J. N. 1995 Linear Robust Control. Prentice-Hall.
- GUSTAVSSON, L. H. & HULTGREN, L. S. 1980 A resonanace mechanism in plane Couette flow. J. Fluid Mech. 98, 149–159.
- Hu, H. H. & Bau, H. H. 1994 Feedback control to delay or advance linear loss of stability in planar Poiseuille flow. Proc. R. Soc. Lond. A 447, 299–312.
- JOSHI, S. S., SPEYER, J. L. & KIM, J. 1995 Modelling and control of two dimensional Poiseuille flow. 34th IEEE Conf. on Decision and Control, pp. 921–927.
- JOSHI, S. S., SPEYER, J. L. & KIM, J. 1997 A systems theory approach to the feedback stabilization of infinitesimal and finite-amplitude disturbances in plane Poiseuille flow. J. Fluid Mech. 332, 157–184.
- JOSLIN, R. D., GUNZBURGER, M. D., NICOLAIDES, R. A., ERLEBACHER, G. & HUSSAINI, M. Y. 1997 Self-contained automated methodology for optimal flow control AIAA J. 35, 816–824.
- KAILATH, T. 1980 Linear Systems. Prentice-Hall.
- KHORRAMI, M. R., MALIK, M. R. & ASH R. L. 1989 Application of spectral collocation technique to the stability of swirling flows *J. Comput. Phys.* 81, 206–229.
- Kim, J., Moin, P. & Moser, R. 1987 Turbulence statistics in fully developed channel flow at low Reynolds number. J. Fluid Mech. 177, 133–166.
- Laub, A. J. 1991 Invariant subspace methods for the numerical solution of Riccati equations. In *The Riccati Equation* (ed. Bittaini, Laub, & Willems), pp. 163–196. Springer.
- LEWIS, F. L. & SYRMOS, V. L. 1995 Optimal Control. Wiley.
- Moin, P. & Bewley, T. R. 1995 Application of control theory to turbulence *Twelfth Australasian Fluid Mechanics Conf.*, Dec. 10–15, Sydney, 109–117.

- Orszag, S. A. 1971 Accurate solution of the Orr–Sommerfeld stability equation *J. Fluid Mech.* **50**, 4, 689–703.
- Orszag, S. A. & Patera, A. T. 1983 Secondary instability of wall-bounded shear flows *J. Fluid Mech.* 128, 347–385.
- REYNOLDS, W. C. & KASSINOS, S. C. 1995 One-point modeling of rapidly deformed homogeneous turbulence *Proc. R. Soc. Lond.* A **451**, 87–104.
- Skogestad, S. & Postlethwaite, I. 1996 Multivariable Feedback Control. Wiley.
- Trefethen, L. N., Trefethen, A. E., Reddy, S. C. & Driscoll, T. A. 1993 Hydrodynamic stability without eigenvalues *Science* **261**, 578–584.
- ZHOU, K., DOYLE, J. C. & GLOVER, K. 1996 Robust and Optimal Control. Prentice-Hall.